Carbohydrate Polymers 327 (2024) 121684

Contents lists available at ScienceDirect

Carbohydrate Polymers

journal homepage: www.elsevier.com/locate/carbpol

Design of bioactive and biomimetic scaffolds based on chitosan-alginate polyelectrolyte complexes for tissue engineering

Clarissa Ciarlantini [a], Iolanda Francolini [a], Ilaria Silvestro [a], Alessia Mariano [b], Anna Scotto d'Abusco [b], Antonella Piozzi [a,*]

[a] Department of Chemistry, Sapienza University of Rome, P.le A. Moro 5, 00185 Rome, Italy
[b] Department of Biochemical Sciences, Sapienza University of Rome, P.le Aldo Moro 5, 00185 Rome, Italy

ARTICLE INFO

Keywords:
Chitosan
Sodium alginate
Polyelectrolyte complexes
Bioactive and biomimetic scaffolds
3,4-Dihydroxyhydrocinnamic acid
Heparin

ABSTRACT

The replacement and regeneration of biological tissues by fabricating three-dimensional functionalized constructs that can improve material interaction with cells is an important challenge of tissue engineering. In this study, bioactive and biomimetic scaffolds based on chitosan-alginate polyelectrolyte complexes (PECs) were fabricated by freeze-drying method and then crosslinked with $CaCl_2$. Various chitosan-alginate (CS-AL) molar ratios were used to obtain PECs with different structural and mechanical properties. The CS_1-$AL_{2.3}$ scaffold showed to possess the best mechanical properties (8 MPa) and good pore morphology with an average size of 100–150 μm. After the crosslinking process, a less porous structure but with higher elastic modulus (30 MPa) was obtained. To make matrix bioactive and biomimetic, the CS_1-$AL_{2.3}$ system was first functionalized with 3,4-dihydroxyhydrocinnamic acid (HCAF) and then with $PySO_3$ or Heparin to introduce groups/molecules mimicking the extracellular matrix. While the antioxidant properties of the scaffolds containing HCAF improved by 3 orders of magnitude, compared to the non-functionalized matrix, the introduction of sulfonic groups into the bioactive scaffold made the structure more porous and hydrophilic with respect to the heparinized one also favoring the penetration and proliferation of fibroblasts into the scaffold. These results indicate the potential of these novel systems for tissue engineering.

1. Introduction

The biological activity of certain tissues can be limited by trauma, aging or disease. In these cases, the functionality of the tissue must be restored. To this end, in recent years, the recovery of damaged tissue/organ has been the most used solution. Tissue engineering (TE) studies the design and construction of bioreactors and involves the application of active cells seeded on three-dimensional porous supports named scaffolds with the aim of controlling stimulation and growth factors of cells and producing biological substitutes that could be implanted in the defect (Chan & Leong, 2008; Zhao et al., 2016).

To fabricate synthetic extracellular matrices possessing high porosity and, at the same time, able to maintain the mechanical properties necessary to restore the structure and composition of the target tissue is one of the main challenges of TE (Bombaldi de Souza et al., 2019; Choi, Zhang, & Xia, 2010). The material constituting the scaffold must also possess biological properties such as biocompatibility, biodegradability and bioactivity (Stratton, Shelke, Hoshino, Rudraiah, & Kumbar, 2016). Among various biomaterials which can be used in the fabrication of scaffolds (O'Brien, 2011), polysaccharides play a crucial role thanks to their structural and functional similarities to the extracellular matrix (ECM) (Sood, Gupta, & Agrawal, 2021; Tchobanian, Van Oosterwyck, & Fardim, 2019). Particularly, Chitosan (CS) is extensively studied for TE applications due to its tuneable chemical and biological properties that can promote cell adhesion and proliferation. However, although this polymer is an exceptional material from the point of view of biocompatibility, it does not permit to control the degradation phase and often has a low mechanical resistance. Compression modulus values from 50 to 200 KPa for chitosan (CS) scaffolds have been reported in several studies (Albanna, Bou-Akl, Walters, & Matthew, 2012; Xu et al., 2017; Xu & Simon, 2005). To enhance the stability in aqueous environment and mechanical properties, chitosan-based systems are generally crosslinked with formation of covalent or ionic bonds among polymer chains (Wahba, 2020). However, the crosslinking reaction cannot lead

* Corresponding author.
E-mail address: antonella.piozzi@uniroma1.it (A. Piozzi).

https://doi.org/10.1016/j.carbpol.2023.121684
Received 4 October 2023; Received in revised form 6 December 2023; Accepted 8 December 2023
Available online 11 December 2023

to much improvement in mechanical properties. Fang, Zhang, Song, and Sun (2020) performed the cross-linking of collagen/chitosan scaffolds with glutaraldehyde (GTA), genipin (GP) or tripolyphosphate (TPP) improving the dimensional stability of the systems in aqueous medium but reaching relatively high compressive modulus (CM) values, up to 614 KPa, only in the case of the scaffolds crosslinked with GTA. While interpenetrating polymer network hydrogels composed of chitosan and photo-crosslinkable gelatin, developed by Suo et al. showed compressive modulus values of maximum 116 KPa (Suo et al., 2018). Good mechanical properties were instead achieved by our group using both an open structure, manufactured by exploiting a thermally induced phase separation of chitosan solutions, then stabilized by freeze-gelation and photo crosslinking (CM 2.2 MPa), and a simple ionic crosslinking of scaffolds fabricated employing different concentrations of CS and TPP as well as various crosslinking reaction times (CM from 0.2 to 4.7 MPa) (Silvestro et al., 2020, 2021). Improved mechanical properties for CS can also be achieved by introducing nanostructured fillers within the polymer matrix. Various nanomaterials (natural and synthetic polymers, metals and ceramics) have been widely used for tissue engineering (Zheng et al., 2021). For example, systems based on CS and hydroxyapatite, or CS, silica, and polycaprolactone, have been employed in regeneration of dental tissues (Mortazavi, Mehdikhani Nahrkhalaji, Fathi, Mousavi, & Nasr Esfahani, 2010), bone (Liu et al., 2013), and nervous tissues (Boni, Ali, Shavandi, & Clarkson, 2018). However, drawbacks as poor interfacial interaction between polymer chains and nanomaterial, and inhomogeneous dispersion of nanomaterial itself in the scaffold could limit the specific application. Nanostructured cellulose was also employed as a reinforcement in composite materials for different applications. Particularly, cellulose nanocrystals, bacterial nanocellulose, and cellulose nanofibrils have been shown to have great potential both alone and in nanocomposite polymer matrices for biomedical applications, including TE. In this last decade, numerous reviews and manuscript have been published on characteristics and properties of nanocellulose and its applications in the medical field (Bacakova et al., 2019; Jorfi & Foster, 2015; Nicu, Ciolacu, & Ciolacu, 2021). The increasing interest towards these green nanomaterials is due to their excellent mechanical properties, low cost, renewability and biocompatibility. The combination of cellulosic nanomaterials with CS has led to the successful fabrication of scaffolds for skin, bone, cartilage and hydrogels for wound dressings (Khan, Wang, & Ni, 2020). However, although nanocellulosic materials are very promising in different fields, further investigations are need to overcome some challenges concerning their potential toxic- or side-effects on human health and high industrial production cost.

Another strategy to overcome the low mechanical resistance of CS lies in the formation of polyelectrolyte complex-based structures (PECs). PECs are formed by ionic interactions between cationic and anionic polymers (Raj, Kumar Sharma, & Malviya, 2018). As reported in literature, PECs based on natural polymers are widely used in TE as they allow to modulate the structural properties of the system by varying the concentration of polymers and the production method (Bhardwaj & Kundu, 2011; Ng, Yeong, & Naing, 2016; Sæther, Holme, Maurstad, Smidsrød, & Stokke, 2008). Different polyanions have been investigated to fabricate CS-based PECs including pectin, hyaluronic acid, dextran sulfate, sodium alginate (Potaś, Szymańska, & Winnicka, 2020). However, electrostatic interactions alone are often not sufficient to make such systems biostable in an aqueous environment. Therefore, also in this case, a covalent or physical crosslinking using low molecular weight molecules is considered a useful approach (Chen et al., 2010; Meng et al., 2021; Patil, Saha, & Biswas, 2017).

Sodium alginate (AL), another polysaccharide widely used in biomedical applications, is constituted by (1–4)-linked β-d-mannuronic acid (M units) and (1–4)-linked α-l-guluronic acid (G units) residues. AL possesses gel-forming ability in presence of multivalent cations (Agulhon, Markova, Robitzer, Quignard, & Mineva, 2012; Zheng, 1997). Gelation process takes place by ionic interactions between cations and carboxyl groups of G units present on the polymer chain, which are stacked to form an egg-box-like structure (Grant, Morris, Rees, Smith, & Thom, 1973). The use of CS-AL polyelectrolyte complexes has proved to be a valid strategy to improve the poor mechanical properties of CS alone or crosslinked CS (Fang et al., 2020). Unlike CS, AL is not a good substrate for cells and protein as it is a negatively charged polymer (Qin, 2008).

Although enormous progress has been made in the preparation of polymeric scaffolds, many studies are still needed to improve their biological properties as well as to achieve a good cell-matrix interaction. In fact, cells present into the matrix can undergo oxidative stress deriving from physiological imbalance between antioxidants and oxidants (free radicals or reactive oxygen species, ROS) in favor of oxidants (Picardo & Dell'Anna, 2010). Oxidative stress leads to the inactivation of metabolic enzymes or damage of important cellular components (Simon, Haj-Yehia, & Levi-Schaffer, 2000; Tyagi, Gambhir, Kumar, Gangenahalli, & Verma, 2021). High molecular weight CS has a moderate antioxidant activity due to the formation of intramolecular hydrogen bonds which prevent the hydroxyl and amino groups from carrying out their radical scavenger action. Such antioxidant activity increases with the molecular weight decreasing thanks to the enhanced solubility of CS oligomers that make active the aforementioned functional groups (Abd El-Rehim, El-Sawy, Hegazy, Soliman, & Elbarbary, 2012; Feng, Du, Li, Hu, & Kennedy, 2008). The introduction of antioxidant molecules into scaffolds by functionalization of CS could be a winning strategy to obtain bioactive matrices to be used in TE (Bagheri, Validi, Gholipour, Makvandi, & Sharifi, 2022; Bergonzi et al., 2021; Radwan-Pragłowska et al., 2018; Shaik & Kowshik, 2019). Even the preparation of a biomimetic matrix able to recall the chemical structure of the natural ECM can improve cell-device interaction (Naik & Singamaneni, 2017; Patterson, Martino, & Hubbell, 2010). Indeed, as ECM is formed by glycosaminoglycans containing negatively charged groups and fibrous proteins, the functionalization of chitosan or the introduction of molecules containing carboxylated and/or sulfonated groups or components of ECM could favor the cell-scaffold interaction. In literature, over the last twenty years, different works have reported the manufacture of biomimetic chitosan systems resulting from its modification with sulfonate groups (Dimassi, Tabary, Chai, Blanchemain, & Martel, 2018, Han et al., 2020; Jiang et al., 2022; Wang et al., 2019; Zhou et al., 2009). Given the functionalities of chitosan, the obtained polymers can present unreacted amino groups, sulfate, and sulfonate groups. These polyampholytic features make sulfonated and/or sulfate chitosan derivatives similar to sulfate glycosaminoglycans present in ECM. Therefore, they are promising candidates for various biomedical applications, including TE. Chitosan biomimetic composite scaffolds containing hydroxyapatite, collagen, hyaluronic acid or heparin have also been fabricated (Cheng et al., 2021; Gümüdereliolu & Aday, 2011; Haag, Dalton, & Bloemen, 2022). Thein-Han and Misra (2009) developed CS-hydroxyapatite nanocomposite scaffolds for which pre-osteoblasts adhesion and proliferation were significantly improved than the pure chitosan scaffold, while Lin, Tan, Marra, Jan, and Liu (2009) evaluating the performance of scaffolds obtained by using different ratios of collagen/hyaluronic acid/chitosan demonstrated that the presence of ECM components favored the proliferation of fibroblasts cultured in the tri-copolymer porous structures. Also loading of heparin and nerve growth factor onto CS scaffolds fabricated using lyophilization method enhanced the attachment and proliferation of Schwann cells, promoting peripheral nerve generation (Li, Xiao, Zhang, Zhao, & Yang, 2017).

In this framework, the present study aims to fabricate polysaccharide-based scaffolds by freeze-drying method starting from PECs formed by CS and AL. The scaffolds were manufactured by employing different molar ratios between CS and AL to evaluate their influence on mechanical properties and morphological structure of the systems. In order to obtain bioactive PECs, the most performing system was chemically modified with 3,4-dihydroxyhydrocinnamic acid (HCAF) and then crosslinked with calcium ions (Ca^{2+}). In particular,

HCAF was bonded to the scaffold via a reaction in-solution carried out with an enzymatic catalyst, laccase. Such a functionalization lead to the formation of a covalent bond between the antioxidant and the polymer system which did not affect the functional groups responsible for the biological activity of the molecule. Afterwards, to make the matrix bioactive also biomimetic, the system was reacted with the sulfur trioxide pyridine complex ($PySO_3$) or heparin (HEP). In particular, the procedure for synthesizing sulfonated chitosan was developed to be performed in a heterogeneous phase and to further promote the N-sulfation reaction, avoiding depolymerization phenomena caused by high reaction temperatures. In this study, papers focused on strategies employed to obtain bioactive and/or biomimetic scaffolds published in the last 20 years were reviewed. To the best of our knowledge, no studies have been conducted aimed at covalently binding an antioxidant to CS-AL scaffolds and simultaneously inserting functional groups (-COOH and/or -SO_3H) potentially stimulating cell adhesion and proliferation. All of the obtained systems were studied by thermal, mechanical and spectroscopic analyses as well as swelling measurements. The morphological characteristics of the scaffolds, in term of porosity and pore interconnectivity, were evaluated by scanning electron microscope observations and porosity measurements. The successful introduction of the antioxidant molecule was verified by the ninhydrin test, while the DPPH model radical was used to determine the antioxidant activity of the systems after the coupling process between PECs and HCAF. Finally, for the most promising scaffolds, preliminary biocompatibility studies with fibroblast cells were carried out.

2. Materials and methods

2.1. Materials

Chitosan from shrimp shell with molecular weight 190–310 KDa, viscosity 200–800 cps and 75–85 % deacetylation degree (Silvestro et al., 2020), sodium alginate from *Macrocystis pyrifera* with molecular weight 132–320 KDa, viscosity 5.0–40.0 cps, guluronic content of 44 %, determined by ^{1}H NMR (Murtas et al., 2005), and Laccase from *Trametes Versicolor* with a nominal activity of 1.06 U/mg protein were purchased from Sigma Aldrich and used as received. Other chemicals were of analytical grade and purchased from Sigma-Aldrich.

2.2. Preparation of chitosan-alginate PEC scaffolds

CS solution at 3 % (w/v) was prepared by dissolving a correct amount of polymer powder in 20 mL of acetic acid solution (2 % v/v). With the same procedure, sodium alginate solutions were prepared at different concentrations, specifically 3, 4, 5 % (w/v), by dissolving AL in 30 mL of a sodium hydroxide solution (1 N). Each of these solutions was mixed with that of CS and kept under constant stirring for 24 h to obtain a homogeneous chitosan–alginate solution. Considering the repetitive unit of the two polymers, 3 different CS and AL molar ratios (1:1.2, 1:1.75 and 1:2.3), corresponding to weight ratios of 1:1.5, 1:2 and 1:2.5, were investigated. After stirring, the pH of the chitosan-alginate solutions was adjusted to 7.4 by adding 2 N acetic acid dropwise.

Hence, 3 mL of each solution was poured into cylindrical plastic molds, frozen at −20 °C overnight and then freeze-dried for 24 h. The obtained scaffolds were crosslinked with a 3 % w/v $CaCl_2$ solution for 30 min, washed with deionized water (DI) twice and then left to soak for 1 h to remove unbound $CaCl_2$. Finally, the samples were freeze-dried for 8 h.

Acronyms used for the systems were: CS_1-$AL_{1.2}$, CS_1-$AL_{1.75}$ and CS_1-$AL_{2.3}$ for the pristine chitosan-alginate scaffold and CS_1-$AL_{2.3}$-$CaCl_2$ for the crosslinked one.

2.3. Introduction of 3,4-dihydroxyhydrocinnamic acid (HCAF) into chitosan-alginate PEC system

According to the procedure followed by I. Brzonova et al., the grafting of phenolic molecules on the chitosan-alginate PEC was performed using laccase enzyme (Brzonova, Steiner, Zankel, Nyanhongo, & Guebitz, 2011). In our case, the functionalization reaction was carried out directly on the solution of chitosan-alginate PEC, as described above. Specifically, the chitosan-alginate PEC solution (50 mL) was added to a 3,4-Dihydroxyhydrocinnamic acid (HCAF) aqueous solution to obtain a final concentration of 10 mM HCAF. The reaction was then started by adding 0.5 mL of laccase (20 nkat mL^{-1} in 2 mL of 50 mM sodium citrate buffer at pH 4.5) and left for 11 h at 30 °C under stirring at 150 rpm. After the functionalization reaction, 3 mL of the solution was poured into cylindrical plastic molds, frozen at −20 °C overnight and then lyophilized for 24 h. The obtained scaffold was crosslinked with a 3 % w/v $CaCl_2$ solution for 30 min, washed extensively with DI water and then left to soak for 3 h to remove excess $CaCl_2$ and the unbound phenolic molecules. The sample was then freeze dried for 8 h. The acronym used for the functionalized and crosslinked scaffold was CS_1-$AL_{2.3}$-HCAF-$CaCl_2$.

2.4. Heparin introduction into chitosan–alginate-HCAF scaffold

According to a procedure reported in literature (Gümüdereliolu & Aday, 2011), heparin conjugation procedure involved the activation of its carboxyl groups by 1-ethyl-3-(3-dimethylaminopropyl)carbodiimide (EDC) and *N*-hydroxysuccinimide (NHS) to form a covalent bond between the amino groups of CS and the carboxyl groups of heparin. EDC and NHS in a molar ratio of 0.6 were added to a 2 % (w/v) solution of heparin (HEP) in 0.05 M MES buffer (2-(*N*-morpholino)ethanesulfonic acid, pH 5.0). After 15 min, the functionalized scaffold (CS_1-$AL_{2.3}$-HCAF-$CaCl_2$) was immersed into that solution. The reaction was left to proceed for 4 h at 37 °C. Afterwards, the heparinized CS_1-$AL_{2.3}$-HCAF-$CaCl_2$ scaffold was extensively washed with DI water, frozen at −20 °C and then freeze-dried for 8 h. Acronym used for the heparinized scaffold was CS_1-$AL_{2.3}$-HCAF-$CaCl_2$-HEP.

2.5. Sulfonation of the chitosan-alginate-HCAF scaffold

The sulfonation reaction was carried out on the preformed CS_1-$AL_{2.3}$-HCAF-$CaCl_2$ scaffold, using the sulfur trioxide pyridine complex ($PySO_3$), which can react with -OH and -NH_2 groups of CS and -OH of AL, giving rise to a pyridonium salt. To further promote the N-sulfation reaction and avoid depolymerization phenomena caused by high reaction temperature, the procedure to synthesize sulfonated chitosan used by Zhou et al. (2009) was modified to be performed in a heterogeneous phase. Briefly, the scaffold was immersed in a solution of $PySO_3$, obtained by dissolving the reagent in 20 mL of *N*, *N*-Dimethylformamide (DMF), in a ratio of 3/1 with respect to –OH and 2/1 to -NH_2 groups of the two polysaccharides. Since the $PySO_3$ adduct can undergo hydrolysis, the reaction was carried out in an anhydrous environment under nitrogen flow. The reaction was left for 1 h at 0 °C and for 6 h at room temperature. Then, the functionalized scaffold was treated with sodium hydroxide (1 N) to free the sulfate groups from the pyridine. Subsequently, the matrix was subjected to washing cycles in DMF to totally remove the sodium salt of pyridine and then with bidistilled water for 12 h, continuously changing the washing solutions. Finally, the scaffold was frozen again in freezer at −20 °C and then freeze-dried for 8 h. Acronym used for this scaffold was CS_1-$AL_{2.3}$-HCAF-$CaCl_2$-SO_3.

2.6. Infrared spectroscopy (FTIR)

The crosslinking and functionalization reactions were evaluated by Fourier Transformed Infrared Spectroscopy (FTIR). Spectra were acquired in attenuated total reflection (ATR) by a Nicolet 6700 (Thermo

Fisher Scientific, Waltham, MA, USA) equipped with a Golden Gate single reflection diamond ATR accessory at a resolution of 2 cm^{-1} and co-adding 200 scans.

2.7. Determination of the functionalization degree of the chitosan-alginate scaffolds

CS amino groups remaining the functionalization reactions were determined by ninhydrin assay (NHN) (Mi, Tan, & Liang, 2001). Briefly, after preparation of a ninhydrin solution at 2 % (w/v) in 2-isopropanol, 12 mg of the functionalized scaffold was inserted in 2 mL of ninhydrin solution and left to react at 90 °C for 15 min, using a refrigerant system. During this time, the solution takes on a deep purple color, related to the reaction between ninhydrin and free amino groups. Then, the solution was left to cool for 20 min after which the absorbance was measured at 570 nm using a UV–Vis spectrophotometer (HP DIODE ARRAY, Agilent Technologies Inc., Palo Alto, USA). The concentration of free NH_2 groups in the scaffolds was determined using a calibration curve obtained plotting CS concentration (mg/mL) versus absorbance. The functionalization degree (FD) was estimated by subtracting the concentration of NH_2 groups remaining after functionalization (C_1) from the concentration of those initially present in the non-functionalized scaffold (C_2) divided by the initial concentration of amino groups (C_2).

$$\%FD = \frac{(C_2 - C_1)}{C_2} \times 100 \quad (1)$$

2.8. Scanning electron microscopy (SEM)

The morphology and pore size of the freeze-dried scaffolds were studied by field emission scanning electron microscopy (FESEM, AURIGA Carl Zeiss AG, Oberkochen, Germany). In addition to the external surface, also the bulk structure of the scaffolds was observed after their fracturing by immersion in liquid nitrogen. The samples were gold sputtered before observation. The pore size and homogeneity were obtained by observation of the sample bulk.

2.9. Determination of the scaffold porosity and interconnection degree

A liquid displacement method was used to determine the pore size and interconnectivity of the scaffolds. In particular, a sample with weight W_0 and volume V_0 was plunged in 10 mL of ethanol (density 0.789 g/cm^3 at 20 °C) for 30 min. Since swelling phenomena have to be avoided in this experiment, a suitable liquid must be selected. After that time, the scaffold was removed and weighted (W_1). The interconnected porosity (ε %) was determined by employing the following eq. (Han, Zhou, Yin, Yang, & Nie, 2010):

$$\varepsilon\% = \left(\frac{W_1 - W_0}{\rho_{EtOH} \times V_0}\right) \times 100 \quad (2)$$

Three porosity experiments were performed for each sample and data were reported as average value ± standard deviation.

2.10. Thermal and mechanical characterization

Thermogravimetric analysis (TGA) was carried out employing a Mettler TG 50 thermobalance (Mettler Toledo, Columbus, OH, USA). For analysis, a temperature ramp with a heating rate of 10 °C·min^{-1} under N_2 flow in the temperature range 25–500 °C was used.

Mechanical properties of the scaffolds were studied by compressive tests using an ISTRON 4502 instrument (Instron Inc., Norwood, MA, USA). In particular, the cylindrical samples (diameter of 2 cm and height of 3 cm) were placed between the two Instron flat plates using a 2 kN load cell and a constant deformation rate of 1 mm/min for the measurements. The measurements were carried out at 25 °C temperature and with 40 % humidity. The value of the compressive modulus (CM) was obtained using the linear portion of the stress-strain curve (<10 % of deformation). Five experiments were performed for each sample. The results were reported as average value ± standard deviation.

2.11. Water-uptake kinetics of scaffolds

The water uptake (W) of the scaffolds was determined by immersion of weighted scaffolds (W_0) in phosphate (PBS) buffer (pH 7.4) at room temperature and constant humidity. The scaffold was weighted (W_t) at different times after lightly blotting it on a filter paper to remove excess of liquid. Water uptake was defined as follows:

$$W\% = \left(\frac{W_t - W_0}{W_0}\right) \times 100 \quad (3)$$

For each sample, three experiments were performed, and data were reported as average value ± standard deviation.

2.12. Determination of the antioxidant activity by DPPH method

The evaluation of the antioxidant activity of pure HCAF and CS-AL-HCAF conjugates was carried out using 2,2-diphenyl-1-picrylhydrazyl (DPPH) as a radical model, according to the method developed by Marsden Blois and subsequently modified by Brand-Williams, Cuvelier, and Berset (1995).

In the case of pure HCAF, the antioxidant activity was measured in a homogeneous solution by testing different concentrations of antioxidant molecule. Starting from a 1×10^{-4} M solution of HCAF in methanol, different aliquots were placed in contact with fixed volumes of DPPH (4 mL), at a concentration equal to 0.2 mM. The prepared solutions were left under stirring for 30 min, time necessary to reach the plateau. At the end, the absorbance of the solutions was measured at a wavelength of 520 nm. The concentration of DPPH in the reaction medium was calculated by a calibration curve obtained by measuring the absorbance of DPPH solutions with respect to the concentration of the model radical.

Furthermore, the percentage of residual DPPH in the steady state for each antioxidant concentration was also traced from the calibration curve. By restoring the percentage of residual DPPH to the steady state as a function of the molar ratio between antioxidant and DPPH, it is therefore possible to trace the antiradical activity. This was defined as the amount of antioxidant necessary to reduce the initial concentration of DPPH by 50 % (efficient concentration = EC_{50} (g/L)). The radical scavenging activity was therefore obtained graphically by the value that the curve assumes at 50 % of DPPH at the steady state. As for the functionalized scaffolds, the samples in a variable amount between 0.2 and 20 mg were placed in contact with the same volume of DPPH. After a contact time of 30 min, the absorbance at 520 nm was detected. In this case, the EC_{50} value was obtained by plotting the percentage of residual DPPH at steady state with respect to the ratio between the amount of sample (g) and DPPH volume (L). Therefore, it was defined as the grams of matrix needed to obtain the 50 % residual steady-state DPPH.

2.13. Cell viability assay and adhesion analysis

Human dermal primary fibroblasts were isolated as previously reported (Lopreiato et al., 2020). Then, cells were cultured in Dulbecco's modified Eagle's medium (DMEM) supplemented with 10 % fetal bovine serum (FBS), 1 % penicillin/streptomycin, 1 % L-glutamine, 1 % Na-pyruvate and 1 % non-essential amino acids (Sigma-Aldrich, Co. Saint Louis, MO, USA) at 37 °C and 5 % CO_2.

To study the suitability of the scaffolds to cultivate human fibroblast cells, cell viability tests were performed. In brief, scaffolds (1 cm diameter) were set down into 24 well tissue culture plate and then, cells were added into the wells at a density of 5×10^4 cells/well and cultured for 48 h at 37 °C and 5 % CO_2. As control, cells were seeded into a plate well without sample. After incubation time, the viability of cells seeded

on the scaffolds as well as the cells growth on the wells was quantified by measuring the mitochondrial dehydrogenase activity using the MTS dye. The culture media was removed, and scaffolds were put into a clean well. Then, 300 μL MTS dye solution was added in each well and cells were incubated for 3 h to allow the formation of soluble formazan crystals by viable cells. Color variation was monitored as cell viability and measured at 492 nm using a multi-plate reader (NeBiotech, Holden, MA, USA). All the measurements were performed in triplicate.

The adhesion of cells seeded onto scaffolds was observed by a Leica DM IL LED optical microscope, using an AF6000 modular microscope (Leica Microsystem, Milan, Italy m). A total of 5×10^4 fibroblasts were seeded onto scaffolds as described above and incubated for 48 h. At the end of this incubation time, the scaffolds containing the cells were washed in PBS, fixed in 4 % paraformaldehyde in PBS for 15 min at 4 °C, and permeabilized with 0.5 % Triton-X 100 in PBS for 10 min. Then, cellular proteins were blocked with 3 % bovine serum albumin in PBS for 30 min, and then stained with DAPI to visualize the nuclei. All these steps were performed at RT.

2.14. Statistics

Analysis of variance comparisons was performed using Mini-Tab. Differences were considered significant for $p < 0.05$. Data are reported as means ± SD.

3. Results and discussion

Several materials have been investigated to develop scaffolds for TE, including inorganic composites, natural and synthetic polymers (Collins et al., 2021). Polymers are largely employed in the medical field since their chemical-physical properties can be easily modified to fulfill different applications. The main advantage of synthetic polymers is reproducible large-scale production with controlled properties of strength, degradation, and microstructure. Among synthetic polymers, the most commonly used in TE are aliphatic polyesters such as polylactide (PLA), polyglycolide (PLG) and their copolymers (Slomkowski, 2007). However, a low cell adhesion and proliferation was evidenced for these polymers due to poor cell-material interaction caused by their hydrophobicity and lack of functionality for chemical modifications (Lee, Song, Jegal, & Kimura, 2013; Pellegrino et al., 2017). On the contrary, natural polymers have the advantage of molecular recognition, biodegradation, resemblance to the extracellular matrix and chemical flexibility make them materials of choice for several medical applications (Abbasian, Massoumi, Mohammad-Rezaei, Samadian, & Jaymand, 2019).

CS is a cationic polysaccharide widely used for several biomedical applications (Vunain, Mishra, & Mamba, 2017) including TE thanks to its non-toxicity, biocompatibility, biodegradability and hydrophilic nature which can promote cell adhesion and avoid negative effects unrelated to the implant (Islam, Biswas, Sakib, & Ur, 2020). However, CS-based scaffolds are mechanically weak and particularly unusable in load-bearing applications. Improvement of mechanical and structural properties of CS scaffolds has been achieved by ionic or covalent crosslinking, or by formation of composites with fillers and synthetic or natural polymers (Bhardwaj & Kundu, 2011; Francolini et al., 2019; Ng et al., 2016; Silvestro et al., 2020). In particular, biostable and mechanically resistant structures can be obtained by exploiting the ionic interactions between CS and an anionic polyelectrolyte, such as sodium alginate, with subsequent gelation by using divalent cations.

In this work, to obtain systems with different porosity and mechanical properties, scaffolds with various CS:AL molar ratios (see Table 1) were fabricated by ionotropic gelation and then crosslinked with calcium chloride (Liling et al., 2016; Russo, Malinconico, & Santagata, 2007).

From the results of the physical characterization, discussed further on, the scaffold with the ratio CS:AL 1:2.3 resulted the most promising in terms of morphology, porosity, thermal stability, and mechanical properties. Therefore, this scaffold has been considered for further functionalization.

Table 1
Acronyms and physical properties of CS-AL scaffolds. T_D = degradation temperature; CM = compressive modulus; EC_{50} = efficient concentration; FD = functionalization degree. The scaffolds were crosslinked with 3 % (w/v) $CaCl_2$ concentration, while a 10 mM HCAF concentration was used for the functionalization reaction.

Sample	T_D (°C)	CM (MPa)	EC_{50} (g/L)	Pore size (μm)	FD (%)
CS_1-$AL_{1.2}$	240	2.22 ± 0.03	3200 ± 60	20–110	–
CS_1-$AL_{1.75}$	252	3.31 ± 0.02	3250 ± 75	40–200	–
CS_1-$AL_{2.3}$	257	8.30 ± 0.03	3270 ± 45	80–240	–
CS_1-$AL_{1.2}$-$CaCl_2$	230	4.82 ± 0.03	3340 ± 33	30–70	–
CS_1-$AL_{1.75}$-$CaCl_2$	243	7.60 ± 0.02	3370 ± 44	50–140	–
CS_1-$AL_{2.3}$-$CaCl_2$	240	30.02 ± 0.02	3400 ± 60	80–180	–
CS_1-$AL_{2.3}$-HCAF-$CaCl_2$	245	37.05 ± 0.04	1.62 ± 0.04	50–130	12
CS_1-$AL_{2.3}$-HCAF-$CaCl_2$-SO_3	255	33.02 ± 0.03	1.65 ± 0.02	100–350	23
CS_1-$AL_{2.3}$-HCAF-$CaCl_2$-HEP	237	40.04 ± 0.02	5.26 ± 0.01	40–100	30

Indeed, to make the system bioactive, the CS_1-$AL_{2.3}$ scaffold was first functionalized with an antioxidant (HCAF, Fig. 1a) using laccase as a catalyst (Brzonova et al., 2011) and then crosslinked with Ca^{2+}. Finally, to improve the bioactivity and emulate ECM, two different scaffold functionalization strategies were used. The first one involved a sulfonation reaction of the crosslinked CS_1-$AL_{2.3}$-HCAF system by using the sulfur trioxide-pyridine complex (PySO3) (the mechanism is shown in Fig. 1b). In the second strategy, heparin was bound to the amino groups of CS after activation of its carboxylic groups with EDC:NHS (Gümüdereliolu & Aday, 2011) (Fig. 1c). As mentioned above, for the first time, CS-AL based PECs were covalently functionalized with both an antioxidant and groups or molecule potentially stimulating cell adhesion and proliferation.

All the produced samples with relative acronyms are reported in Table 1.

3.1. Infrared spectroscopy analysis

To evaluate the formation of the polyelectrolyte complexes, the FTIR-ATR spectra of the CS-AL scaffolds with different molar ratios were displayed in Fig. 2A and compared with those of pristine chitosan and alginate. As reported by Brugnerotto et al. (Brugnerotto et al., 2001) the spectrum of CS shows the presence of the following characteristic bands: a broad absorption between 3500 and 3000 cm^{-1}, corresponding to -OH and -NH stretching frequencies; the C—H stretching in the range 2920–2875 cm^{-1}; the C = O stretching of acetylate groups (amide I) at 1650 cm^{-1}; the N—H bending of primary amine together with N—H in plane deformation (amide II) and C—N stretching at 1560 cm^{-1}; absorptions due to the pyranose ring in the range 1150–1000 cm^{-1}, particularly the C-O-C and C-O-H stretching at 895 cm^{-1}. As regards AL, the following characteristic absorptions could be observed: the stretching of -OH groups in the region between 3600 and 3000 cm^{-1}; the CH_2 stretching at 3000–2850 cm^{-1}; the C═O stretching vibrations of the carboxyl group in the range between 1600 and 1400 cm^{-1}: the COO^- antisymmetric and symmetrical stretching at 1590 cm^{-1} and 1421 cm^{-1}, respectively. In addition, it was possible to identify the presence of C-O-C and C—O stretching bands between 1300 and 950 cm^{-1}.

By comparing the spectra of the various CS-AL scaffolds with those of

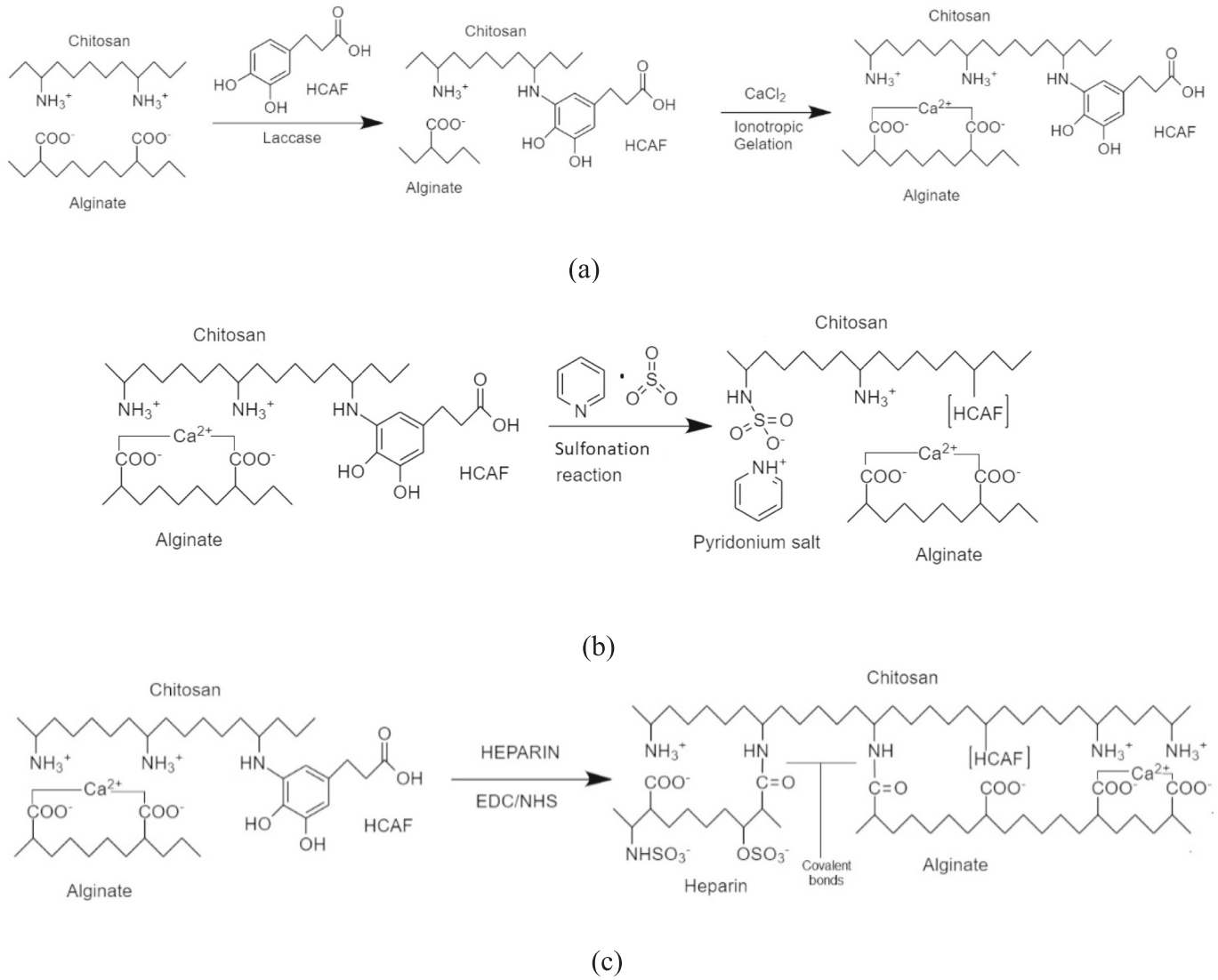

Fig. 1. Functionalization of CS_1-$AL_{2.3}$ polyelectrolyte complex with HCAF and subsequent crosslinking reaction with CaCl2 **(a)**; with $PySO_3$ **(b)** and heparin (HEP) (c).

the uncontaminated CS and AL, some differences were observed due to the formation of the polyelectrolyte complexes. In particular, in the spectra of the composite scaffolds, a narrower and more intense band could be highlighted at 3250 cm^{-1}, caused by the formation of new hydrogen bonds between the -OH and -NH_2 groups of CS and the -C=O and -OH groups of AL. Moreover, a decrease in the absorption of the antisymmetric COO- stretching and the shift of this band from 1590 cm^{-1} to 1540 cm^{-1} as well as the decrease of the peak related to the amino group at 1173 cm^{-1} were observed in the spectra of PECs compared to that of AL. All of these variations could be traced back to the interaction between the carboxylic groups of alginate and the amine groups of chitosan. In literature, to confirm the formation of chitosan-alginate PECs, different IR absorptions have been considered. For example, Wang et al. (2019) observed new peaks at about 1620 and 1530 cm^{-1}, assigned to the carboxylic groups of the alginate associated with the chitosan and to the amino groups of chitosan associated with the alginate, respectively. Li, Ramay, Hauch, Xiao, and Zhang (2005) attributed the increase in the absorption of the II amide band, the shift of the I band of the amide from 1643 to 1654 cm^{-1} and the absence of the peak at 1173 cm^{-1} to the formation of the CS-AL polyelectrolyte complex. Finally, Lawrie et al. (2007), using FTIR and X-ray photoelectron spectroscopy as complementary techniques, evidenced that it was difficult to observe significant changes in PECs spectra compared to those of individual polymers. These authors demonstrated that FTIR technique alone is not sufficient to identify the presence and extent of interactions between the carboxylic groups of the alginate and the amino groups of chitosan. However, in our study, IR variations observed in the spectra of PECs appeared to be evident and a function of increasing AL concentration. Indeed, the intensity decrease of the antisymmetric COO^- stretching, its shift to lower wavenumbers and the decrease of the peak relating to the amino group at 1173 cm^{-1} could be attributed to the increase in the interaction of -NH_3^+ (chitosan) with -COO^- (alginate) with increasing AL concentration. In addition, a new peak at 1700 cm^{-1} was visible in the spectra of PECs with a 1:1.75 and 1:2.3 CS:AL molar ratio. This absorption could be attributed to the formation of dimeric structures involving two carboxylic groups of adjacent chains as the concentration of AL increased. In the spectra of the CS_1-$AL_{1.75}$ and CS_1-$AL_{2.3}$ scaffolds, this conformational rearrangement was confirmed by the presence at about 1640 cm^{-1} of the C=O stretching of acetylate groups (amide I) of CS. All of this could suggest that the amino groups interested in interacting with the carboxyl groups of AL increased with AL increasing concentration.

To evidence the functionalization of the matrices in Fig. 2B, the spectra of the CS_1-$AL_{2.3}$ scaffold and its derivatives were reported.

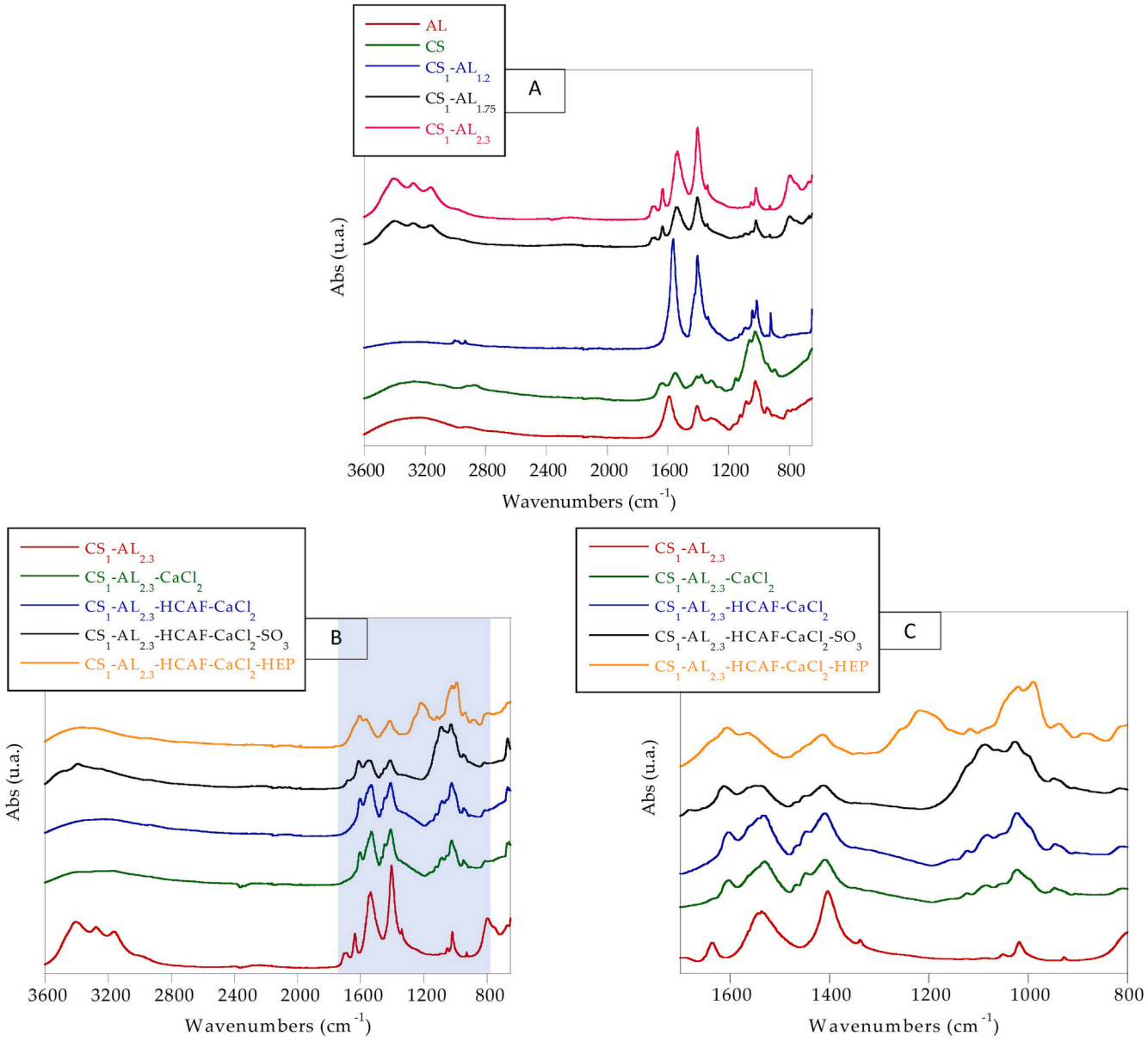

Fig. 2. FTIR spectra of pristine chitosan (CS) and alginate (AL), and of the 3 different prepared PECs **(A)**; FTIR spectra of CS_1:$AL_{2.3}$ molar ratio and subsequently crosslinked and modified matrices **(B)**; magnification of the region from 800 to 1700 cm^{-1} **(C)**.

Several changes in the spectrum were observed after the crosslinking process of the CS-AL scaffold. Indeed, it was possible to observe the disappearance of the peak at 1700 cm^{-1}, relating to the formation of dimeric structures between alginate adjacent chains, and the appearance of a new band at 1620 cm^{-1}, resulting from the union of the band relating to the COO- antisymmetric stretching of the alginate (1590 cm^{-1}) and those of amide I and II of CS (1640 and 1560 cm^{-1}, respectively). The shifts of these latter bands were probably due to the greater contribution of the vibrations inherent in the amino groups of CS left free following the reaction of the calcium ions with carboxyl groups of the alginate and to the formation of a greater number of hydrogen bonds involving the C═O of acetyl groups. Furthermore, the decrease of the COO^- symmetric stretching peak (1420 cm^{-1}) and the consequent increase of the bands in the range 1150–1000 cm^{-1}, attributed to the stretching vibrations of the C-O-H, C-O-C and C—N bonds, were observed. Also, the band at 3250 cm^{-1}, which indicated the formation of new hydrogen bonds between the -OH and $-NH_2$ groups of CS, and the -C═O and -OH groups of AL, showed a decrease in intensity and a broadening of the peak. These changes, ascribed to the loss of hydrogen bonds caused by interactions established between the carboxyl groups and the Ca^{2+} cation, highlighted the successful crosslinking of the matrix and the formation of the "egg box" structure. As for the introduction of the antioxidant molecule, the scaffold spectrum after the HCAF functionalization did not show significant differences compared to that of the unmodified scaffold. Probably, the absorption peaks related to the antioxidant were covered by those of PEC. On the contrary, the sulfonation reaction and heparin introduction provoked substantial changes in the spectra of the functionalized PECs. In the case of sulfonation, the spectrum was characterized by the variation of the absorption in the region between 1000 and 1200 cm^{-1} and the formation of a pronounced peak in the range between 1100 and 1200 cm^{-1} due to the symmetrical stretching of the SO_2 groups. These results are in agreement with those reported by Sun, Shi, Wang, Fang, and Huang (2017). The same absorption was evidenced in the spectrum of the scaffold after HEP reaction (between 1160 and 1260 cm^{-1}), as reported by Ho, Mi, Sung, and Kuo (2009). In addition, an increase of the band at 1650 cm^{-1} was

observed due to the formation of ionic and chemical interactions between the protonated amino groups and the deprotonated carboxyl groups of HEP.

3.2. Determination of the functionalization degree of the chitosan-alginate scaffolds

To determine the functionalization degree of the scaffolds, ninhydrin test was used (Mi et al., 2001).

From the data reported in Table 1, it was noted that the introduction of the antioxidant molecule caused a decrease of about 12 % of the concentration of the free amino groups with respect to the non-functionalized matrix, suggesting the successful formation of the bond between the CS amino groups and HCAF. After the introduction of sulfonate groups and heparin, a further decrease of the free amino group concentration of 11 % and 18 % respectively, was determined. This evidenced that the sulfonation reaction occurred not only with the -OH groups of CS but also with those amino ones; while as for the heparinized matrix, the use of EDC and NHS reagents led to formation of amidic bonds between CS and heparin or CS and AL, as shown in Fig. 1C.

3.3. Thermogravimetric analysis

Thermal analysis of scaffolds can provide insight on the formation of PEC structures. In fact, the thermal stability of PECs depends on the interactions that are generated between the two polymers. Furthermore, parameters such as thermal stability and decomposition temperature (T_d) are influenced by the crosslinking process (Gubanova et al., 2021). In Table 1, the degradation temperatures of all the tested matrices are shown, while in Fig. 3A, the thermogravimetric curves of the scaffolds obtained at different CS:AL molar ratios compared to those of the two starting polymers are reported. In all thermograms, it was possible to observe a first weight loss around 100–120 °C attributed to elimination of bound water and a second one between 250 and 300 °C due to the degradation of the polymers constituting the scaffolds. The T_d values of the two homopolymers were 285 °C and 240 °C for CS and AL respectively. Interestingly, the formation of CS-AL polyelectrolyte complexes and their functionalization disturbed the ordered structure of CS, decreasing its thermal stability (see data in Table 1). Differently from what reported by Lin et al., as the amount of AL increased the T_d of PECs increased, highlighting an enhancement in ionic interactions between the two polymers (Lin & Yeh, 2010). These data, in agreement with FT-IR analysis, demonstrated that the sample with a CS:AL molar ratio of 1:2.3 was the one in which the formation of the polyelectrolyte complex was more effective.

For this reason, and for the mechanical analysis, whose results will be discussed later, the CS_1-$AL_{2.3}$ scaffold was chosen for the subsequent functionalization.

The T_d value of the CS_1-$AL_{2.3}$-$CaCl_2$ scaffold, whose thermogram is shown in Fig. 3B, was lower than that of the non-crosslinked matrix CS_1-$AL_{2.3}$. Presumably, the electrostatic interactions between the COO^- groups of AL and Ca^{2+} cations disturbed the already formed interactions between AL and CS.

The successful introduction of HCAF into the crosslinked scaffold was evidenced by an increase in the T_d value (245 °C) compared to that of the non-functionalized sample (240 °C). This was probably due to the formation of hydrogen bonds between the antioxidant molecule and polymer chains. A considerable improvement in the thermal stability of the CS_1-$AL_{2.3}$-HCAF-$CaCl_2$ matrix was noted after the subsequent introduction of the sulfonated groups. In this case, the higher stabilization was attributed to the formation of more hydrogen bonds and ionic interactions between the introduced $-SO_3$ groups and the polymer chains, which made the CS structure more compact. On the contrary, the introduction of HEP led to a decrease in the degradation temperature (T_d=237 °C) ascribed to a reduction of the interactions between the two polysaccharides owing to the formation of amidic bonds between –COOH and $–NH_2$ groups of HEP and CS, respectively.

3.4. Morphological properties and porosity tests

In order to promote cell adhesion and proliferation, scaffolds must have an appropriate mean pore size to be used successful in TE (Choong, 2013; Vikingsson, Claessens, Gómez-Tejedor, Gallego Ferrer, & Gómez Ribelles, 2015). Therefore, the study of the pore size and their distribution is of fundamental importance. Morphological analysis, performed by FESEM, showed that the freeze-drying process is a good method for fabricating porous structures based on CS and AL. Various factors can influence the morphology and porosity of scaffolds obtained by the freeze-drying such as chemical structure and concentration of used polymers, crosslinking degree and type of crosslinking agent, and

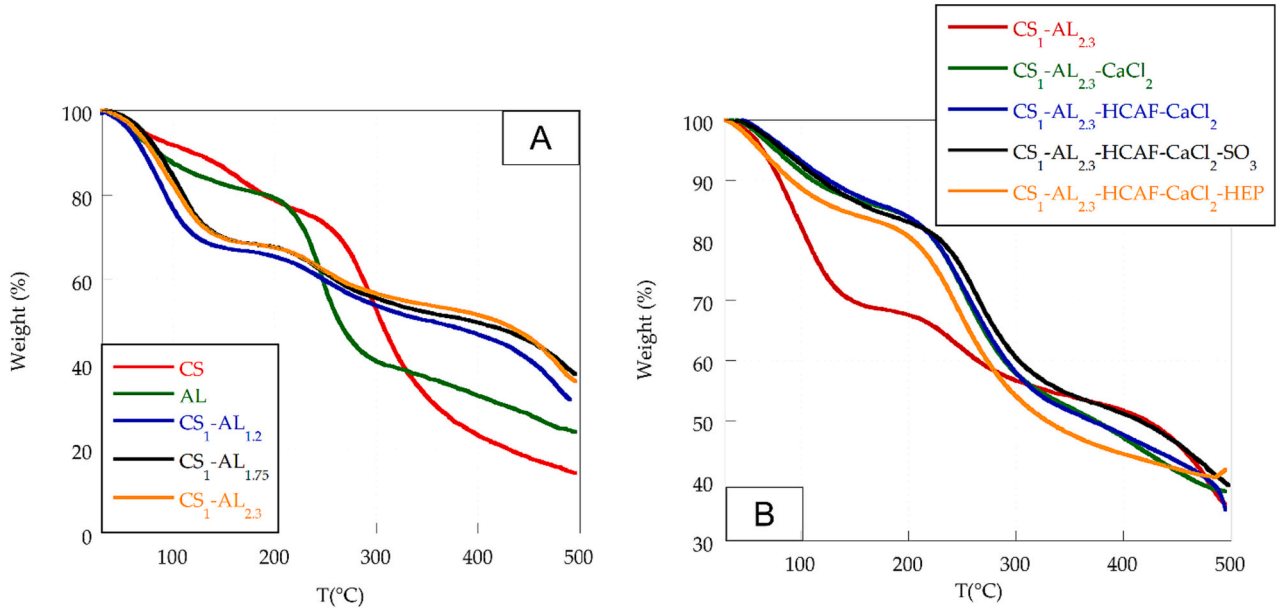

Fig. 3. Thermogravimetric curves of pristine chitosan (CS), pristine alginate (AL) the 3 different molar ratios evaluated (1:1.2–1:1.75–1:2.3) **(A)**; Thermogravimetric curves of 1:2.3 M ratio and subsequently crosslinked and modified matrices **(B)**.

finally, the experimental conditions used for the preparation of the structures (freezing temperature and/or drying process parameters) (Raeisdasteh Hokmabad, Davaran, Ramazani, & Salehi, 2017).

As it can be observed from SEM micrographs (Fig. 4a) and data related to pore size (Table 1), the amount of AL influenced the final morphology of the materials. The CS_1-$AL_{1.2}$ sample had a rather compact structure with irregularly distributed cavities ranging in size from 20 to 110 μm. The morphology of the sample CS_1-$AL_{1.75}$ appeared instead less dense with more homogeneous cavities around 150 μm in size. In the case of the CS_1-$AL_{2.3}$ matrix, pores of larger dimensions (80–240 μm), well distributed and of regular size were highlighted. The increase in pore size with AL increasing amount was probably due to an improved interaction between AL and CS. Indeed, after the phase separation of the PEC solutions, occurred during freezing stage, the porous structure was generated by removal of the solvent. The spaces originally occupied by the solvent became pores in the scaffolds. If the interactions between the two polymers were strong enough to form a sufficiently rigid architecture surrounding the solvent, when the solvent was removed the structure did not collapse and therefore remained porous (Reys et al., 2017). As demonstrated by FTIR and thermal data, the CS_1-$AL_{2.3}$ scaffold was the one that established the more effective interactions between the functional groups of the two polysaccharides.

The crosslinking process caused a decrease in the scaffold volume with a slight collapse of the 3D structure, evidencing the formation of "egg boxes" between AL and Ca^{2+} cations. In the micrograph of the crosslinked CS_1-$AL_{2.3}$, shown in Fig. 5a, a decrease in the size of the pores and an overall more compact structure could be observed.

The introduction of the antioxidant molecule seemed to clearly stabilize the morphology of the matrix. In fact, the sample showed homogeneously distributed pores that did not collapse after the crosslinking process. In this case, the formation of a covalent bond between HCAF and the amino groups of CS, the structural rigidity of the antioxidant and its possibility to establish hydrogen bonds with polymer chains ensured the maintenance of the three-dimensional porous structure even after the crosslinking reaction with calcium chloride and the further freeze-drying phase. As regards the sulfonated matrix, a significant increase in the pore size was observed (around 100–350 μm). Unlike the introduction of the antioxidant, which took place in solution, the sulfonation reaction was carried out in solid phase on the preformed scaffold. In this case, Py-SO_3 reagent managed to diffuse within the structure probably reacting not only with the -NH_2 of the CS (11 % functionalization degree) but also with the -OH of the two polysaccharides. The introduction of very large and negatively charged sulfonate groups therefore led to a greater separation of the polymer chains with consequent increase in pore size. In addition, the sulfonic groups were able to establish hydrogen bonds with the chains stabilizing the modified structure of the scaffold during the freeze drying process. On the contrary, HEP provoked a decrease in the pore size of the scaffold structure (40–100 μm). This result was not in accordance with what was found by Ho et al., who reported a pore size >100 μm after the conjugation reaction between HEP and a CS-AL polyelectrolyte complex (Ho et al., 2009). The difference was probably due to the experimental procedure adopted for the conjugation reaction. In our case, by performing the reaction on the preformed scaffold and not on the gel-form sample, HEP was able to reduce the pore size. Nevertheless, as the fibroblast size is around of 15–20 μm, the heparinized matrix seemed to possess the pore size more suitable for our applications unlike the sulfonated one.

For these materials to be applied successfully, it is of paramount importance to fabricate structures with interconnected pores. Indeed, the cells introduced into the matrix must be supplied with gases and nutrients so that they can proliferate and create new tissue (Landman & Cai, 2007). To determine the interconnection degree (ε %) of the scaffolds, the liquid displacement method was used. In the case of the scaffolds at different CS-AL molar ratios, the pore interconnection

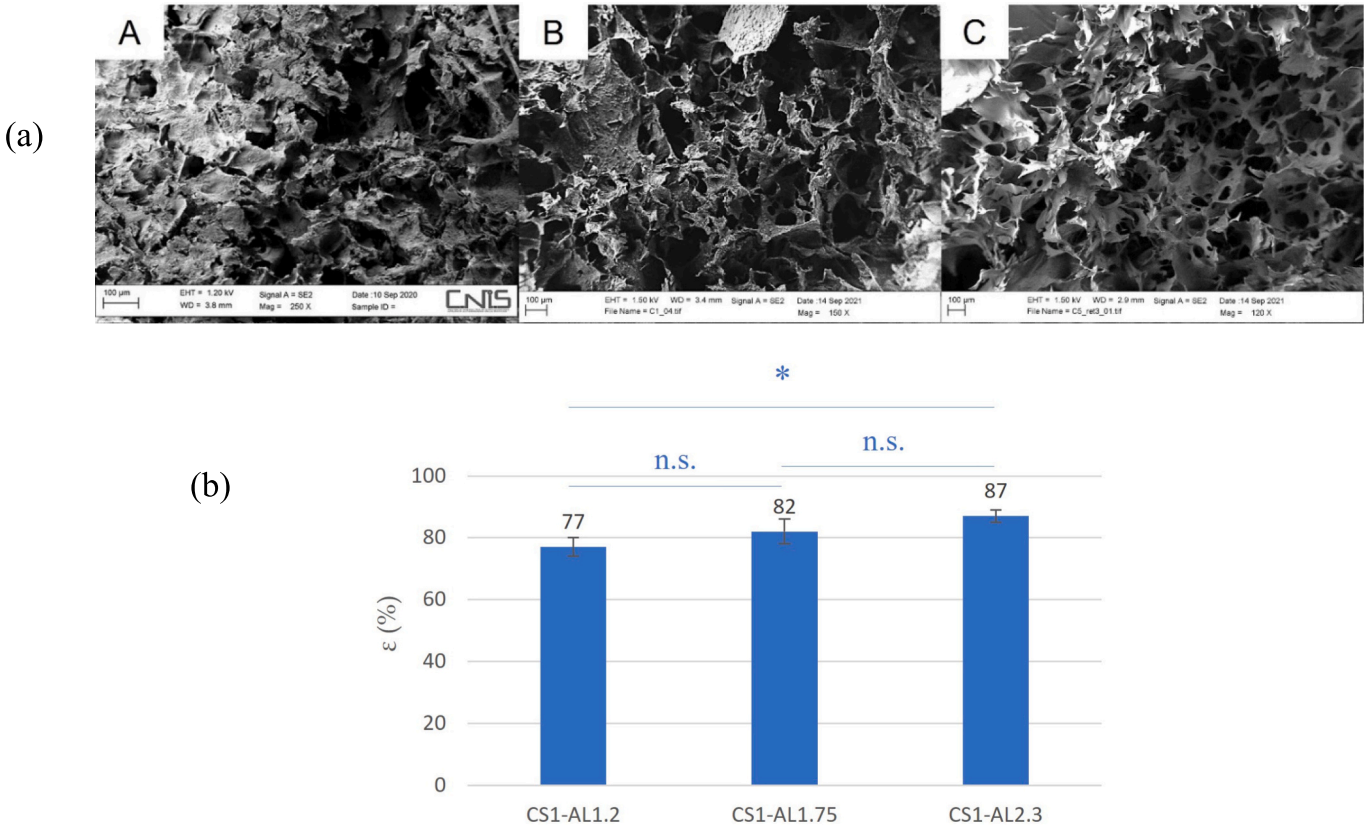

Fig. 4. (a): SEM micrographs of the obtained scaffolds: CS_1-$AL_{1.2}$ (A); CS_1-$AL_{1.75}$ (B); CS_1-$AL_{2.3}$ (C), (b): Interconnected porosity (ε%) of the prepared systems. Statistical analysis showed a significant difference when *p-value < 0.05, n.s. = not significant.

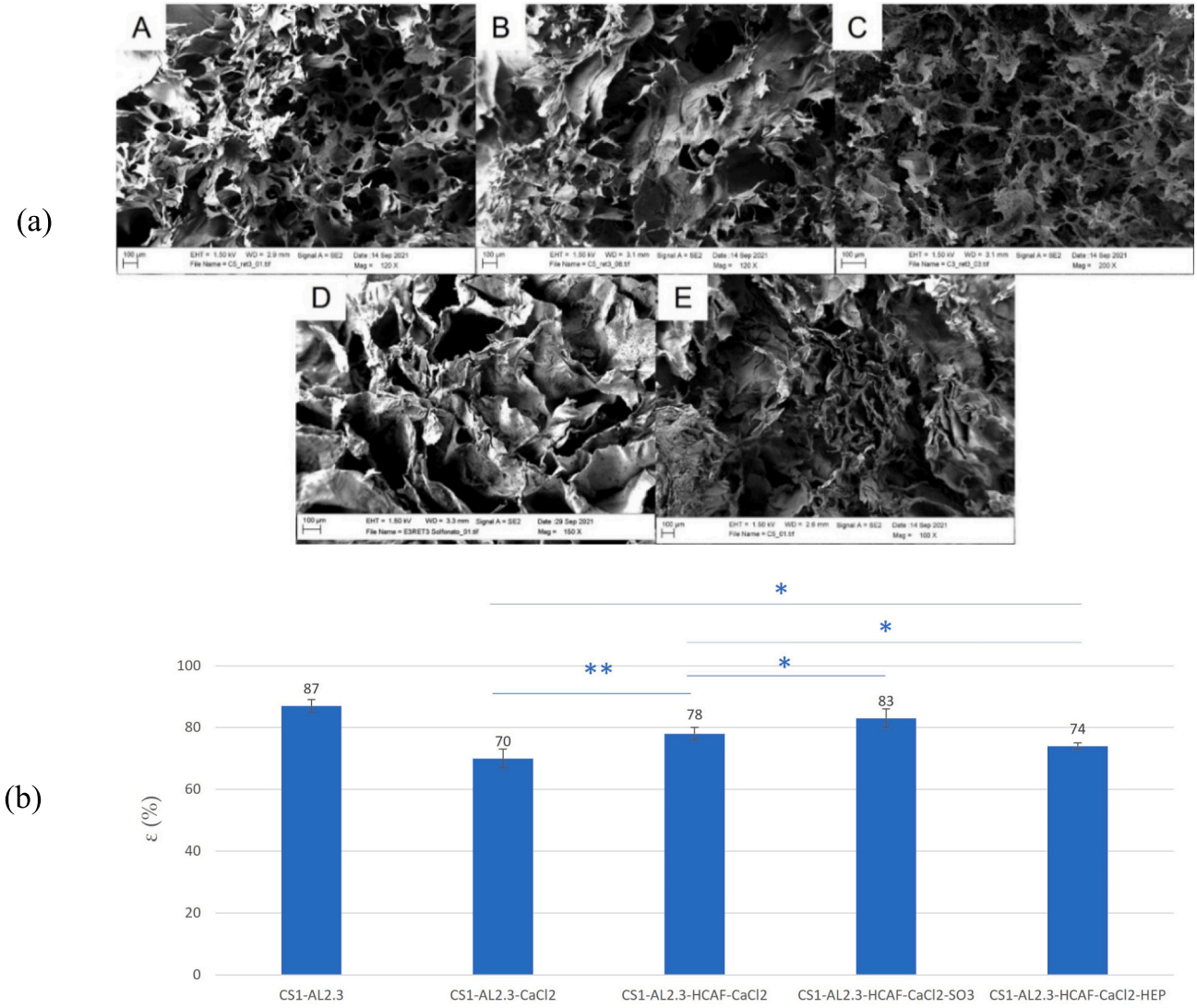

Fig. 5. (a): Scanning Electron Microscopy (SEM) micrographs of the obtained scaffolds: CS_1-$AL_{2.3}$ (A); CS_1-$AL_{2.3}$-$CaCl_2$ (B); CS_1-$AL_{2.3}$-HCAF-$CaCl_2$ (C); CS_1-$AL_{2.3}$-HCAF-$CaCl_2$-SO_3 (*D*) and CS_1-$AL_{2.3}$-HCAF-$CaCl_2$-HEP (E). (b): Interconnected porosity (ε%) of the prepared systems. Statistical analysis showed a significant difference when *p-value < 0.05 and **p-value < 0.01.

degree increased with the alginate concentration increasing (Fig. 4b). Probably, during the freezing phase, in the CS_1-$AL_{2.3}$ system characterized by the greater quantity of AL, rearrangements of polymer chain portion occurred favored by the formation of hydrogen bonds between the chains themselves and the water molecules which led to the construction of a network with more interconnected pores. The same matrix after the crosslinking process with Ca^{2+} cations showed a decrease in the degree of interconnection (Fig. 5b). On the contrary, the introduction of HCAF antioxidant or -SO_3 groups into the scaffold led to a higher degree of pore interconnection compared to the non-functionalized matrix. As previously reported, functionalization of CS with large polar molecules provoked the separation of polymer chains. During the freezing phase, the increased chain mobility favored interactions with water molecules leading to the formation of large and continuous domains of ice crystals which resulted in an enhancement of the pore interconnection. In the case of the system conjugated with HEP a decrease in the degree of interconnection was observed. Probably, the presence of many functional groups in the macromolecule favored the formation of more bonds with the matrix (18 % functionalization degree), leading to a denser structure with reduced porosity. This contributed to less diffusion of water molecules in the three-dimensional structure, resulting in reduced pore interconnection.

3.5. Mechanical properties

Resistance of a material to compression or elongation is of primary importance in TE. In fact, once implanted, the material must have adequate mechanical and functional resistance in accordance with that of the tissue to be replaced. The mechanical properties of the material must therefore be comparable to those of the tissue with which the material will interact (Lv et al., 2010).

The CM values and stress–strain curves of the scaffolds obtained by using different CS:AL molar ratios were reported in Table 1 and Fig. 6A, respectively. To determine the CM value, the slope of the curve until 10 % of deformation was considered. After that deformation, a collapse of the structure was observed causing an increase of the strength value due to the bulk effect of the polymer.

As reported by Yang et al., the value of elastic modulus of the CS matrix alone depends on the polysaccharide concentration and in the case of concentration 1–2 % (w/v) it was around 0.038–0.07 MPa (Yang et al., 2010). These values are not suitable for regeneration of skeleton muscles, that have an elastic modulus around 0.5–3 MPa (Collinsworth, Zhang, Kraus, & Truskey, 2002).

However, by inserting an anionic polymer capable of generating a polyelectrolyte complex, the CS elastic modulus can be significantly

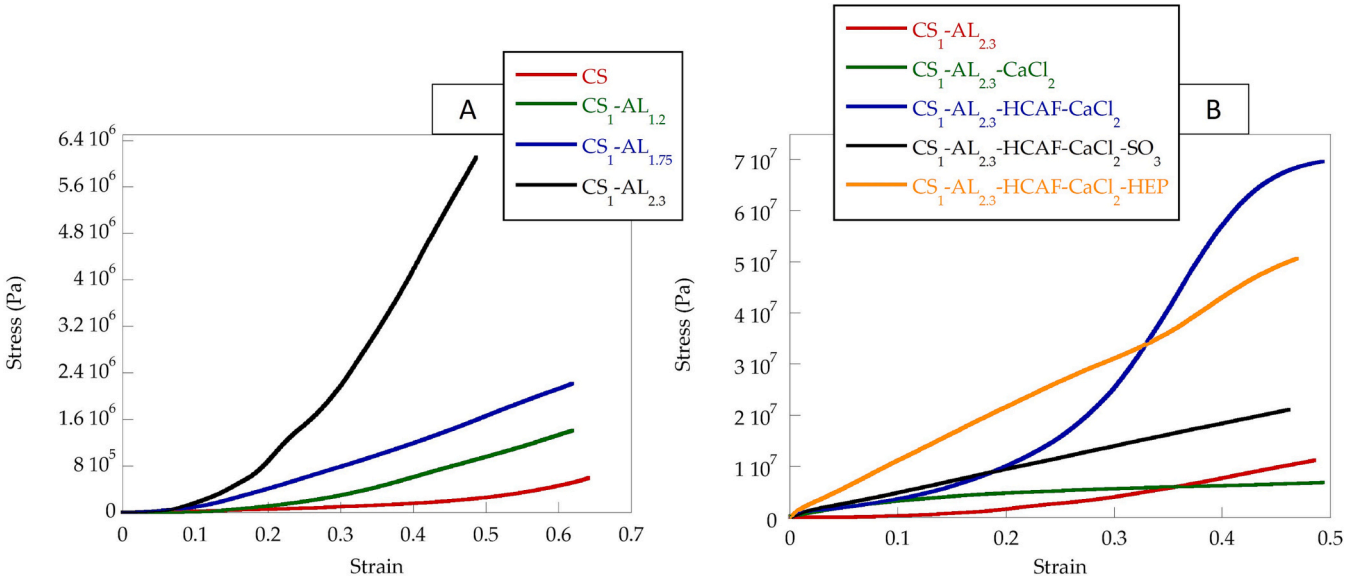

Fig. 6. Stress-strain curves of pristine chitosan and the 3 different molar ratios evaluated (1:1.2–1:1.75–1:2.3) **(A)**; Stress-strain curves of 1:2.3 M ratio and subsequently crosslinked and modified matrices **(B)**.

increased. Li et al. reported a value of the elastic modulus of 8 MPa using a concentration of 2.4 % (w/v) for each of the two polymers (Li et al., 2005). This is because the two polymers forming the polyelectrolyte complex are held together by strong ionic interactions which lead to a more resistant matrix. Furthermore, by increasing the concentration of AL, for the same quantity of CS, it is possible to increase the mechanical properties of PECs. Indeed, in our case, values of the elastic modulus from 2.2 to 8.3 MPa were obtained using a CS concentration of 3 % (w/v) and, of 3, 4 and 5 % (w/v) of AL (see data in Table 1). These results were attributed to a better interaction between two polysaccharides with the AL amount increasing, in agreement with thermogravimetric data. Therefore, it was deduced that the most promising molar ratio of the two polymers for future applications in TE, was of CS:AL 1:2.3, which obtained the best compromise between porous structure and mechanical properties.

To evaluate the effect of the crosslinking reaction and subsequent modification, the stress-strain measurements were carried out on the CS_1-$AL_{2.3}$ modified matrices. The curves obtained were reported in Fig. 6B. The crosslinking step generated a considerable increase in the elastic modulus. This was due to the formation of the egg boxes leading to a more collapsed and smaller volume matrix than the original. This increase was greater than that reported by Li et al. for CS-AL scaffolds (Li et al., 2005). The difference in the value of the elastic modulus was probably due to the different concentration of the two polysaccharides used in the fabrication of the scaffolds, particularly that of AL. The introduction of the antioxidant molecule produced a slight increase in the value of the elastic modulus. This was not consistent with the porosity measurements which showed a more apparently brittle structure after the introduction of HCAF molecule. However, SEM measurements evidenced a smaller pore size of the matrix producing a less fragile structure. The presence of the sulfonate groups led to a slight decrease in the mechanical properties of the CS_1-$AL_{2.3}$-HCAF-$CaCl_2$-SO_3 matrix in accordance with the porosity measurements. In fact, as a consequence the sulfonation reaction, the matrix underwent a structural modification which generated a greater interconnection degree and size of the pores. In the case of the $AL_{2.3}$-HCAF-$CaCl_2$-HEP scaffold, an increase in the elastic modulus was observed related to a more compact and resistant matrix, as demonstrated by previous physical characterization and in agreement with Ho et al. (2009) and Gümüdereliolu and Aday (2011) who reported an increase in the elastic modulus with respect to the CS matrix after the covalent introduction of HEP.

3.6. Water-uptake kinetics

Hydrophilicity is an essential property of systems in contact with biological fluids as it must promote cell adhesion and proliferation. Therefore, the swelling characteristics in water and the structural stability of scaffolds are of primary importance for their use in tissue engineering (Landman & Cai, 2007). Swelling measurements of CS-AL non-crosslinked scaffolds were not carried out due to poor dimensional stability of these polyelectrolyte complexes in an aqueous environment. In the case of the crosslinked samples, the swelling properties were evaluated for an incubation period of about 200 min in simulates physiological conditions (PBS buffer, pH = 7.4).

In Fig. 7, the swelling kinetics for the sample with the best CS:AL molar ratio (CS_1-$AL_{2.3}$-$CaCl_2$) and its derivatives were reported. The introduction of the antioxidant molecule decreased the dimensional stability of the matrix in an aqueous environment. This, in agreement with the porosity measurements, was ascribed to the greater degree of the pore interconnection of the CS_1-$AL_{2.3}$-HCAF-$CaCl_2$ structure. The

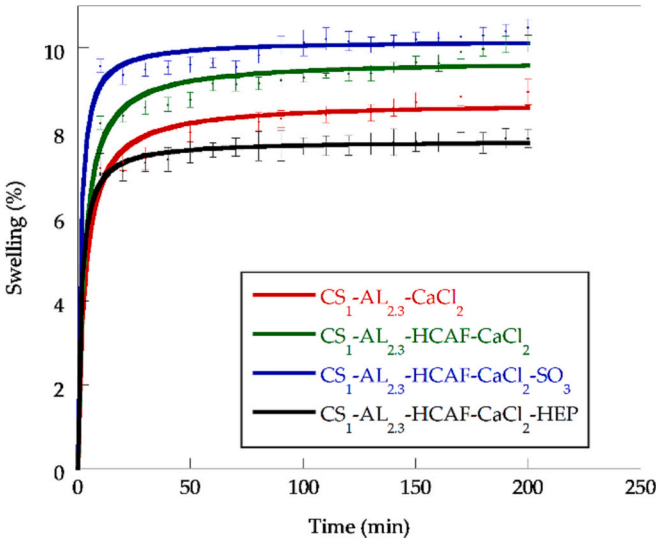

Fig. 7. Swelling kinetics of the crosslinked CS1:AL2.3-$CaCl_2$ scaffold and its derivatives.

same matrix subsequently sulfonated showed the highest swelling capacity. This finding was attributed to the sulfonation reaction that modified the morphology and size of the pores after introduction of the $-SO_3$ bulky groups, as evidenced by the SEM analysis. As a consequence, the hydrophilic groups were more available for interactions with the water molecules. In the case of the CS_1-$AL_{2.3}$-HCAF-$CaCl_2$-HEP sample, the opposite effect was observed with a significant decrease in the swelling capacity of the matrix, as reported by Ho et al. (2009). This is probably due to the clogging of the structure pores by HEP leading to fewer interactions of the matrix with water molecules. This result was confirmed by SEM and porosity measurements which showed a more closed and less interconnected structure.

3.7. Determination of the antioxidant activity by DPPH method

To evaluate the antioxidant properties of the systems, the percentage of DPPH, that remained in the steady state for the functionalized scaffolds, was evaluated with respect to the ratio between the amount of matrix (g) and L of DDPH (see Material and Method section). By comparing the curve of the antioxidant matrices (Fig. 8) and the EC_{50} values shown in Table 1, it was possible to verify whether the bound antioxidant could maintain its radical capture activity (EC_{50} value of HCAF was 0.017 g/L).

By observing the data related to the EC_{50} values, it was possible to note a remarkable improvement in the antioxidant capacity of the matrices functionalized with HCAF and sulfate groups compared to the unfunctionalized CS-AL PECs (Table 1). The values, in fact, decreased by 3 orders of magnitude compared to the non-functionalized matrix. This further demonstrated the successful introduction of the antioxidant molecule and the maintenance of its ability to capture radicals despite the covalent bond with the matrix. In literature, many works have reported the physical incorporation of different antioxidants in CS-based systems. For example, Radwan-Pragłowska et al. (2018), by adding *Tiliaplatyphyllos* to chitosan aerogels highlighted a significant increase in antioxidant properties of the systems compared to the non-functionalized matrix, achieving a DPPH radical removal of 67 %. Shaik and Kowshik (2019) loaded chitosan-collagen scaffolds with different amounts of ellagic acid (from 0.5 to 2 % (w) relative to the weight of the scaffold) observing that the antioxidant potential of the systems increased with increase in antioxidant concentration until reaching radical capture values of approximately 82 %. In our case, HCAF immobilized into the CS_1-$AL_{2.3}$-HCAF-$CaCl_2$ scaffold showed excellent performance (radical capture around 88 %, corresponding to the EC_{50} value = 1.60 g/L) thanks to the formation of a covalent bond with the matrix which did not affect the functional groups responsible for the antioxidant activity of the molecule. In the case of the bioactive and biomimetic scaffolds, CS_1-$AL_{2.3}$-HCAF-$CaCl_2$-SO_3 and CS_1-$AL_{2.3}$-HCAF-$CaCl_2$-HEP, was noted an increase in the EC_{50} value only for the heparinized matrix, due to the decrease in porosity that prevented the antioxidant molecule from interacting with the radicals.

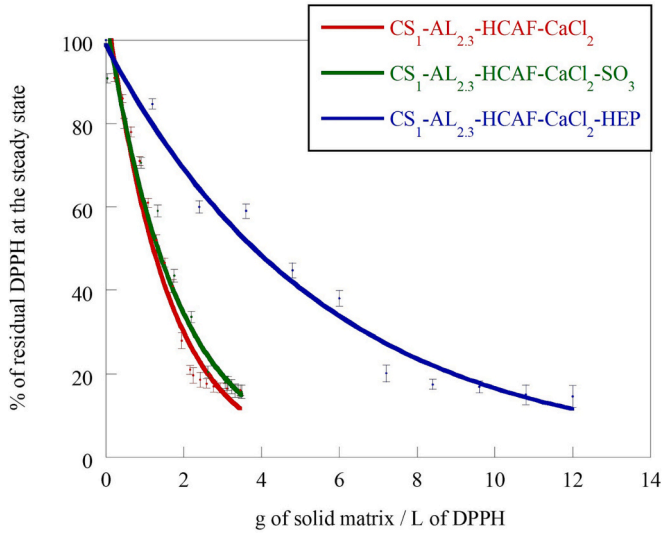

Fig. 8. Decrease in DPPH content as a function of g of solid matrix/L of DPPH.

3.8. Cell viability tests

Finally, to determine the biocompatibility of the systems to consider them as suitable candidates in the TE field, human primary fibroblasts were seeded on their surface and left grown for 48 h. Fig. 9a shows the viability of cells adsorbed on scaffolds compared to the viability of cells seeded in 24-wells of cell culture plates (viability of 100 %). The MTS assay on 48 h-cultured cells confirmed a good biocompatibility of the systems, which proved to be non-toxic against human fibroblasts and not harmful to the cell viability. However, a decrease in viability ($^*p < 0.05$) was detected in the cells cultured on the CS_1-$AL_{2.3}$-$CaCl_2$ scaffold, probably due to the lower number of cells adhered on this support. Instead, the viability percentage of fibroblast cells seeded on HCAF-containing scaffolds was shown to be close to 100 %, probably for the antioxidant molecule protective effect. Shaik and collaborators also verified the positive action of antioxidants on the viability of fibroblast cells after incorporation into CS-based scaffolds of ellagic acid (Shaik & Kowshik, 2019) or Silymarin, active component of the milk thistle plant (Shaik, Dapkekar, Rajwade, Jadhav, & Kowshik, 2019). These bioactive molecules have proven effective in controlling the oxidative stress on cells, following exposure to UV, in a concentration dependent manner, thus promoting cell adhesion and proliferation. In addition, high cell viability on CS aerogels containing a floral extract (Tiliaplatyphyllos) and two aminoacids, used as crosslinkers, was found by Radwan-Pragłowska et al. (2018) who demonstrated that the antioxidant agent enabled high cellular protection against oxidation stress. However, in these systems, as in others reported in the literature, the bioactive molecules were physically introduced into the fabricated scaffolds, while the systems prepared in this work contained the covalently bound antioxidant. Our results demonstrated that the strategy of using an enzyme to immobilize HCAF was successful because the functional groups responsible for the biological action of the molecule were remained free. As no significant difference was observed for the three HCAF-containing samples, to confirm the cellular ability to penetrate and adhere on scaffolds, an immunofluorescence experiment was performed. Unfortunately, it was not possible to observe the morphology of the adhered fibroblasts since the systems tended to absorb the fluorophore used for analysis, making it impossible to detect cells under fluorescence microscopy. However, cellular nuclei were effectively stained with DAPI further confirming the presence of viable cells penetrated the scaffolds (Fig. 9b). Fibroblast cells appeared mostly arranged in groups and their nuclei were large and regular round shaped, thus indicating a good suitability of these materials for the cell growth. Moreover, the amount of observed cells seemed to be higher in the CS_1-$AL_{2.3}$-HCAF-$CaCl_2$-SO_3 and CS_1-$AL_{2.3}$-HCAF-$CaCl_2$-HEP scaffolds compared to the CS_1-$AL_{2.3}$-$CaCl_2$ one, confirming MTS assay findings. The stimulating properties of heparin introduced into CS-based scaffolds on cell adhesion, proliferation and differentiation have been highlighted in many studies. Gümüsderelioglu & Aday reported an increase in pre-osteoblast viability for heparin-functionalized scaffolds (Gümüdereliolu & Aday, 2011). In particular, the authors evidenced that when HEP was covalently immobilized into three-dimensional structures, it induced both cell proliferation and differentiation, while when ionically immobilized it promoted differentiation. HEP is able to bind the basic fibroblast growth factor (bFGF). Indeed, as reported by Ho et al. (2009), the chitosan–alginate PEC scaffold containing a high amount of conjugated heparin and bFGF was able to stimulate the proliferation of HFF (human foreskin fibroblasts) cells differently from the system containing only

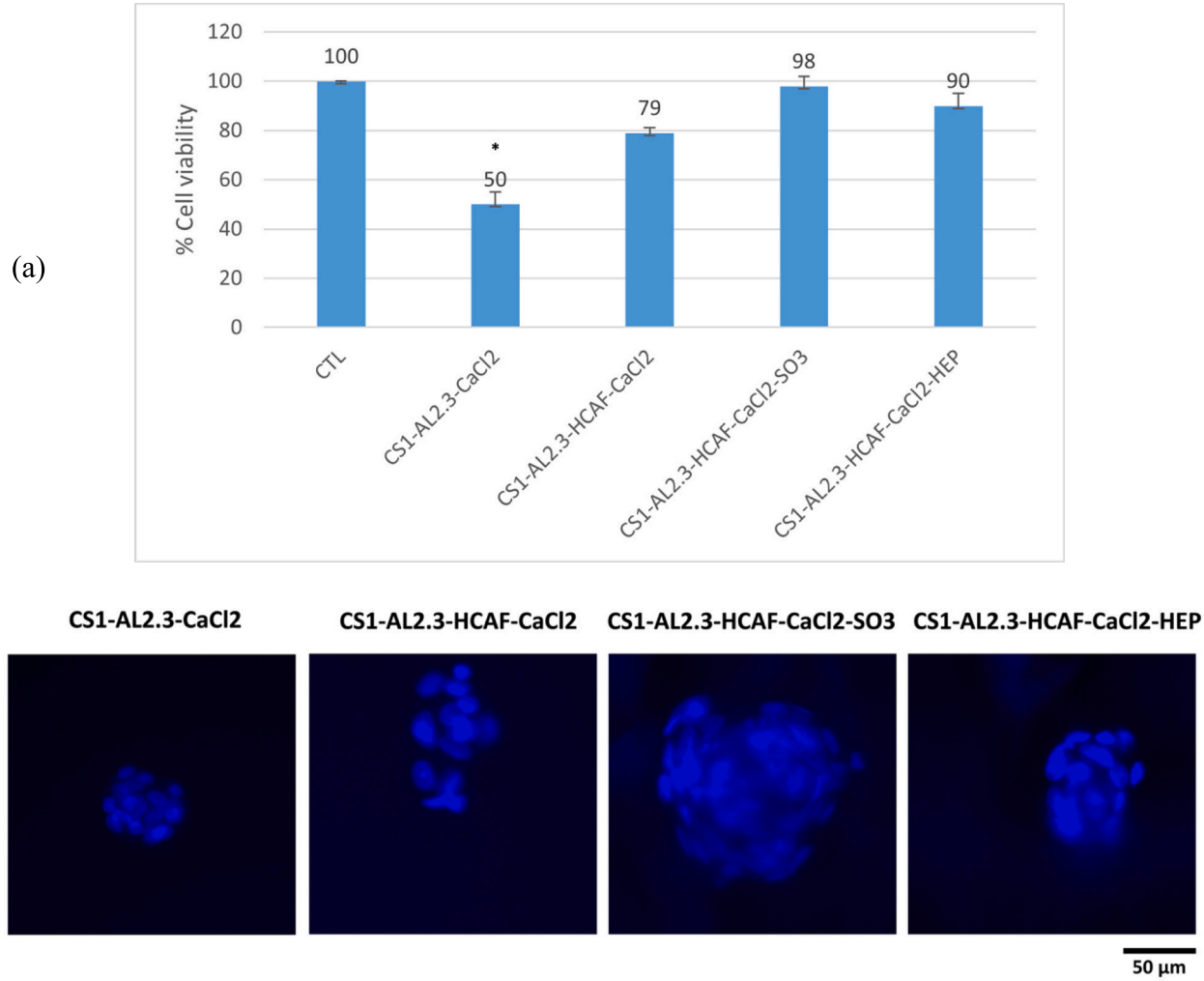

Fig. 9. **(a)** The cell viability of human primary fibroblast seeded onto tested scaffolds was assessed by MTS assay by using cells seeded in 24-well cell culture plate (CTL) as negative control (100 % viability). Results are expressed as mean ± SD of data obtained by three independent experiments, $*p < 0.05$. **(b)** Cell adhesion was visualized by immunofluorescence. Nuclei of cells seeded on scaffolds, and cultivated for 48 h, were stained with DAPI (original magnification 40×).

bFGF. Also scaffolds based on sulfonated or sulfate chitosan (SCS) have been proven to stimulate the proliferation of cells thanks to their heparinoid structure favoring the interaction with biological growth factors. For example, Han et al. (2020) synthesized three type of sulfonated chitosan, 6-O-sulfated chitosan (6-SCS), 2-N-6-O-sulfated chitosan (2,6-SCS) and 3,6-o-sulfate chitosan (3,6-SCS), that proved to be non-toxic and with ability to promote viability and proliferation of human umbilical vein endothelial cells (HUVECs) and to stimulate angiogenesis, especially for the 2,6-SCS derivative. The same result was obtained by Wang et al. (2019) who synthesized two type of hydrogels, 6-O-SCS and 2-N,6-O-SCS hydrogel, formed on the surface of gelatin sponge matrix. The sulfated chitosan-coated scaffolds, particularly the 2-N,6-O-SCS-coated one, demonstrated to be able to capture vascular endothelial growth factor (VEGF) both in vitro and vivo. From immunofluorescence data, it would appear that the functionalization of the bioactive scaffold with sulphonic groups favored the penetration and proliferation of fibroblasts in the scaffold more than that with heparin.

4. Conclusions

The present study investigated the fabrication of scaffolds based on CS-AL polyelectrolyte complexes subsequently crosslinked with Ca^{2+} for the regeneration of skeleton muscle disease. To produce structures suitable for our target, the effect of different molar ratios of the two polysaccharides on the physicochemical properties of the fabricated matrices was studied. FTIR and TGA analyses confirmed the formation of the CS-AL polyelectrolyte complex and indicated the 1:2.3 CS:AL molar ratio as the most effective in the PEC formation. In fact, the best compromise between mechanical properties and pore morphology was achieved for the CS_1-$AL_{2.3}$ scaffold.

The formation of an "egg-box" structure after the ionotropic gelation of the PECs with Ca^{2+} cations, was also confirmed by TGA measurements showed a decrease in the T_d values. Such crosslinking process led to a less porous structure, with a lower interconnection degree of the pores associated with a significant increase in the value of the elastic modulus.

As for the functionalized matrices, ninhydrin test evidenced a functionalization degree of CS with HCAF molecules of 12 %. The introduction of the antioxidant molecule promoted the formation of a more porous structure with more regularity of the pore size. Furthermore, as evidenced by the SEM measurements, the crosslinking process did not provoke a structural collapse of the matrix but left its mechanical strength almost unchanged. The subsequent introduction of biomimetic groups/molecules (sulfonate groups or heparin) led to a substantial change in the morphology of the matrices, as verified by FTIR and TGA analyses. In particular, the introduction of sulfonate groups made the pores larger and more interconnected, causing an increase in the swelling capacity of the matrix and a decrease in the value of the elastic

module. In the case of heparin, an opposite effect was observed. Indeed, heparin clogged the pores and acted as a filler reinforcing increasing the mechanical properties. DPPH test showed a good antioxidant activity of the matrices functionalized with HCAF compared with the non-functionalized one.

Finally, all the scaffolds resulted non-toxic on cell viability, except for the non-functionalized scaffold, CS_1-$AL_{2.3}$-$CaCl_2$, which reduced the viability of the 50 %, whereas the cells seeded on functionalized ones showed almost the same viability compared to cells seeded on plastic devices. It was hypothesized that the lower cell viability for the non-functionalized scaffold could be due to the lower number of cells adhered on the support.

The cell organization inside the scaffolds, observed by nuclei staining, showed the cells grouped and present in larger amount in the functionalized scaffolds, particularly in which functionalized with -SO_3 groups or HEP.

CRediT authorship contribution statement

Clarissa Ciarlantini: Formal analysis, Investigation, Methodology, Writing – original draft. **Iolanda Francolini:** Visualization, Writing – review & editing. **Ilaria Silvestro:** Data curation, Methodology. **Alessia Mariano:** Data curation, Investigation. **Anna Scotto d'Abusco:** Formal analysis, Writing – review & editing. **Antonella Piozzi:** Conceptualization, Supervision, Writing – review & editing.

Declaration of competing interest

The authors declare that they have no financial interests/personal relationships which may be considered as potential competing interests.

Data availability

Data will be made available on request.

Acknowledgments

This work was supported by the Sapienza University of Rome through a grant to A.P. (RM12117A8099E679).

References

Abbasian, M., Massoumi, B., Mohammad-Rezaei, R., Samadian, H., & Jaymand, M. (2019). Scaffolding polymeric biomaterials: Are naturally occurring biological macromolecules more appropriate for tissue engineering? *International Journal of Biological Macromolecules, 134*, 673–694. https://doi.org/10.1016/j.ijbiomac.2019.04.197

Abd El-Rehim, H. A., El-Sawy, N. M., Hegazy, E. S. A., Soliman, E. S. A., & Elbarbary, A. M. (2012). Improvement of antioxidant activity of chitosan by chemical treatment and ionizing radiation. *International Journal of Biological Macromolecules, 50*(2), 403–413. https://doi.org/10.1016/j.ijbiomac.2011.12.021

Agulhon, P., Markova, V., Robitzer, M., Quignard, F., & Mineva, T. (2012). Structure of alginate gels: Interaction of diuronate units with divalent cations from density functional calculations. *Biomacromolecules, 13*(6), 1899–1907. https://doi.org/10.1021/bm300420z

Albanna, M. Z., Bou-Akl, T. H., Walters, H. L., & Matthew, H. W. T. (2012). Improving the mechanical properties of chitosan-based heart valve scaffolds using chitosan fibers. *Journal of the Mechanical Behavior of Biomedical Materials, 5*(1), 171–180. https://doi.org/10.1016/j.jmbbm.2011.08.021

Bacakova, L., Pajorova, J., Bacakova, M., Skogberg, A., Kallio, P., Kolarova, K., & Svorcik, V. (2019). Versatile application of nanocellulose: From industry to skin tissue engineering and wound healing. *Nanomaterials, 9*(2). https://doi.org/10.3390/nano9020164

Bagheri, M., Validi, M., Gholipour, A., Makvandi, P., & Sharifi, E. (2022). Chitosan nanofiber biocomposites for potential wound healing applications: Antioxidant activity with synergic antibacterial effect. *Bioengineering and Translational Medicine, 7*(1), 1–15. https://doi.org/10.1002/btm2.10254

Bergonzi, C., Bianchera, A., Remaggi, G., Ossiprandi, M. C., Zimetti, F., Marchi, C., … Elviri, L. (2021). Biocompatible 3d printed chitosan-based scaffolds containing α-tocopherol showing antioxidant and antimicrobial activity. *Applied Sciences (Switzerland), 11*(16). https://doi.org/10.3390/app11167253

Bhardwaj, N., & Kundu, S. C. (2011). Silk fibroin protein and chitosan polyelectrolyte complex porous scaffolds for tissue engineering applications. *Carbohydrate Polymers, 85*(2), 325–333. https://doi.org/10.1016/j.carbpol.2011.02.027

Bombaldi de Souza, R. F., Bombaldi de Souza, F. C., Rodrigues, C., Drouin, B., Popat, K. C., Mantovani, D., & Moraes, Â. M. (2019). Mechanically-enhanced polysaccharide-based scaffolds for tissue engineering of soft tissues. *Materials Science and Engineering C, 94*(January 2018), 364–375. https://doi.org/10.1016/j.msec.2018.09.045

Boni, R., Ali, A., Shavandi, A., & Clarkson, A. N. (2018). Current and novel polymeric biomaterials for neural tissue engineering. *Journal of Biomedical Science, 25*(1), 1–21. https://doi.org/10.1186/s12929-018-0491-8

Brand-Williams, W., Cuvelier, M. E., & Berset, C. (1995). Use of a free radical method to evaluate antioxidant activity. *LWT - Food Science and Technology, 28*(1), 25–30. https://doi.org/10.1016/S0023-6438(95)80008-5

Brugnerotto, J., Lizardi, J., Goycoolea, F. M., Argüelles-Monal, W., Desbrières, J., & Rinaudo, M. (2001). An infrared investigation in relation with chitin and chitosan characterization. *Polymer, 42*(8), 3569–3580. https://doi.org/10.1016/S0032-3861(00)00713-8

Brzonova, I., Steiner, W., Zankel, A., Nyanhongo, G. S., & Guebitz, G. M. (2011). Enzymatic synthesis of catechol and hydroxyl-carboxic acid functionalized chitosan microspheres for iron overload therapy. *European Journal of Pharmaceutics and Biopharmaceutics, 79*(2), 294–303. https://doi.org/10.1016/j.ejpb.2011.04.018

Chan, B. P., & Leong, K. W. (2008). Scaffolding in tissue engineering: General approaches and tissue-specific considerations. *European Spine Journal, 17*(Suppl. 4). https://doi.org/10.1007/s00586-008-0745-3

Chen, P. H., Kuo, T. Y., Kuo, J. Y., Tseng, Y. P., Wang, D. M., Lai, J. Y., & Hsieh, H. J. (2010). Novel chitosan-pectin composite membranes with enhanced strength, hydrophilicity and controllable disintegration. *Carbohydrate Polymers, 82*(4), 1236–1242. https://doi.org/10.1016/j.carbpol.2010.06.057

Cheng, Y., Morovvati, M. R., Huang, M., Shahali, M., Saber-Samandari, S., Niazi Angili, S., … Toghraie, D. (2021). A multilayer biomimetic chitosan-gelatin-fluorohydroxyapatite cartilage scaffold using for regenerative medicine application. *Journal of Materials Research and Technology, 14*, 1761–1777. https://doi.org/10.1016/j.jmrt.2021.07.052

Choi, S. W., Zhang, Y., & Xia, Y. (2010). Three-dimensional scaffolds for tissue engineering: The importance of uniformity in pore size and structure. *Langmuir, 26*(24), 19001–19006. https://doi.org/10.1021/la104206h

Choong, Q. L. L.a. C. (2013). Three-dimensional scaffolds for tissue engineering applications: Role of porosity and pore size. *Tissue Engineering Part B: Reviews, 19*(6), 1–61.

Collins, M. N., Ren, G., Young, K., Pina, S., Reis, R. L., & Oliveira, J. M. (2021). Scaffold fabrication technologies and structure/function properties in bone tissue engineering. *Advanced Functional Materials, 31*(21), 1–22. https://doi.org/10.1002/adfm.202010609

Collinsworth, A. M., Zhang, S., Kraus, W. E., & Truskey, G. A. (2002). Apparent elastic modulus and hysteresis of skeletal muscle cells throughout differentiation. *American Journal of Physiology - Cell Physiology, 283*(4 52–4), 1219–1227. https://doi.org/10.1152/ajpcell.00502.2001

Dimassi, S., Tabary, N., Chai, F., Blanchemain, N., & Martel, B. (2018). Sulfonated and sulfated chitosan derivatives for biomedical applications: A review. *Carbohydrate Polymers, 202*(August), 382–396. https://doi.org/10.1016/j.carbpol.2018.09.011

Fang, Y., Zhang, T., Song, Y., & Sun, W. (2020). Assessment of various crosslinking agents on collagen/chitosan scaffolds for myocardial tissue engineering. *Biomedical Materials (Bristol), 15*(4). https://doi.org/10.1088/1748-605X/ab452d

Feng, T., Du, Y., Li, J., Hu, Y., & Kennedy, J. F. (2008). Enhancement of antioxidant activity of chitosan by irradiation. *Carbohydrate Polymers, 73*(1), 126–132. https://doi.org/10.1016/j.carbpol.2007.11.003

Francolini, I., Perugini, E., Silvestro, I., Lopreiato, M., Scotto, A., Valentini, F., … Piozzi, A. (2019). Graphene oxide oxygen content affects physical and biological properties of scaffolds based on chitosan/graphene oxide conjugates. *Materials, 12*(1142), 1–17. https://doi.org/10.3390/ma12071142

Grant, G. T., Morris, E. R., Rees, D. A., Smith, P. J. C., & Thom, D. (1973). Biological interactions between polysaccharides and divalent cations: The egg-box model. *FEBS Letters, 32*(1), 195–198. https://doi.org/10.1016/0014-5793(73)80770-7

Gubanova, G. N., Petrova, V. A., Kononova, S. V., Popova, E. N., Smirnova, V. E., Bugrov, A. N., … Skorik, Y. A. (2021). Thermal properties and structural features of multilayer films based on chitosan and anionic polysaccharides. *Biomolecules, 11*(5), 1–15. https://doi.org/10.3390/biom11050762

Gümüderelioglu, M., & Aday, S. (2011). Heparin-functionalized chitosan scaffolds for bone tissue engineering. *Carbohydrate Research, 346*(5), 606–613. https://doi.org/10.1016/j.carres.2010.12.007

Haag, H., Dalton, P. D., & Bloemen, V. (2022). The synergy of biomimetic design strategies for tissue constructs. *Advanced Functional Materials, 32*(32). https://doi.org/10.1002/adfm.202201414

Han, G., Xia, X., Pan, Z., Lin, Y., Li, L., Jiao, Y., Zhou, C., & Ding, S. (2020). Different influence of sulfated chitosan with different sulfonic acid group sites on HUVECs behaviors. *Journal of Biomaterials Science, Polymer Edition, 31*(10), 1237–1253. https://doi.org/10.1080/09205063.2019.1702764

Han, J., Zhou, Z., Yin, R., Yang, D., & Nie, J. (2010). Alginate-chitosan/hydroxyapatite polyelectrolyte complex porous scaffolds: Preparation and characterization. *International Journal of Biological Macromolecules, 46*(2), 199–205. https://doi.org/10.1016/j.ijbiomac.2009.11.004

Ho, Y. C., Mi, F. L., Sung, H. W., & Kuo, P. L. (2009). Heparin-functionalized chitosan-alginate scaffolds for controlled release of growth factor. *International Journal of Pharmaceutics, 376*(1–2), 69–75. https://doi.org/10.1016/j.ijpharm.2009.04.048

Islam, M., Biswas, S., Sakib, N., & Ur, T. (2020). Chitosan based bioactive materials in tissue engineering applications-A review. *Bioactive Materials, 5*(1), 164–183. https://doi.org/10.1016/j.bioactmat.2020.01.012

Jiang, M., Pan, Y., Liu, Y., Dai, K., Zhang, Q., & Wang, J. (June 2021). Effect of sulfated chitosan hydrogel on vascularization and osteogenesis. *Carbohydrate Polymers, 281*, Article 119059. https://doi.org/10.1016/j.carbpol.2021.119059

Jorfi, M., & Foster, E. J. (2015). Recent advances in nanocellulose for biomedical applications. *Journal of Applied Polymer Science, 132*(14), 1–19. https://doi.org/10.1002/app.41719

Khan, A., Wang, B., & Ni, Y. (2020). Chitosan-nanocellulose composites for regenerative medicine applications. *Current Medicinal Chemistry, 27*(28), 4584–4592. https://doi.org/10.2174/0929867327666200127152834

Landman, K. A., & Cai, A. Q. (2007). Cell proliferation and oxygen diffusion in a vascularising scaffold. *Bulletin of Mathematical Biology, 69*(7), 2405–2428. https://doi.org/10.1007/s11538-007-9225-x

Lawrie, G., Keen, I., Drew, B., Chandler-Temple, A., Rintoul, L., Fredericks, P., & Grøndahl, L. (2007). Interactions between alginate and chitosan biopolymers characterized using FTIR and XPS. *Biomacromolecules, 8*(8), 2533–2541. https://doi.org/10.1021/bm070014y

Lee, C. W., Song, B. K., Jegal, J., & Kimura, Y. (2013). Cell adhesion and surface chemistry of biodegradable aliphatic polyesters: Discovery of particularly low cell adhesion behavior on poly(3-[RS]- hydroxybutyrate). *Macromolecular Research, 21*(12), 1305–1313. https://doi.org/10.1007/s13233-013-1181-8

Li, G., Xiao, Q., Zhang, L., Zhao, Y., & Yang, Y. (2017). Nerve growth factor loaded heparin/chitosan scaffolds for accelerating peripheral nerve regeneration. *Carbohydrate Polymers, 171*, 39–49. https://doi.org/10.1016/j.carbpol.2017.05.006

Li, Z., Ramay, H. R., Hauch, K. D., Xiao, D., & Zhang, M. (2005). Chitosan-alginate hybrid scaffolds for bone tissue engineering. *Biomaterials, 26*(18), 3919–3928. https://doi.org/10.1016/j.biomaterials.2004.09.062

Liling, G., Di, Z., Jiachao, X., Xin, G., Xiaoting, F., & Qing, Z. (2016). Effects of ionic crosslinking on physical and mechanical properties of alginate mulching films. *Carbohydrate Polymers, 136*, 259–265. https://doi.org/10.1016/j.carbpol.2015.09.034

Lin, H. Y., & Yeh, C. T. (2010). Alginate-crosslinked chitosan scaffolds as pentoxifylline delivery carriers. *Journal of Materials Science: Materials in Medicine, 21*(5), 1611–1620. https://doi.org/10.1007/s10856-010-4028-2

Lin, Y. C., Tan, F. J., Marra, K. G., Jan, S. S., & Liu, D. C. (2009). Synthesis and characterization of collagen/hyaluronan/chitosan composite sponges for potential biomedical applications. *Acta Biomaterialia, 5*(7), 2591–2600. https://doi.org/10.1016/j.actbio.2009.03.038

Liu, H., Peng, H., Wu, Y., Zhang, C., Cai, Y., Xu, G., … OuYang, H. W. (2013). The promotion of bone regeneration by nanofibrous hydroxyapatite/chitosan scaffolds by effects on integrin-BMP/Smad signaling pathway in BMSCs. *Biomaterials, 34*(18), 4404–4417. https://doi.org/10.1016/j.biomaterials.2013.02.048

Lopreiato, M., Cocchiola, R., Falcucci, S., Leopizzi, M., Cardone, M., Di Maio, V., … Scotto d'Abusco, A. (2020). The glucosamine-derivative NAPA suppresses MAPK activation and restores collagen deposition in human diploid fibroblasts challenged with environmental levels of UVB. *Photochemistry and Photobiology, 96*(1), 74–82. https://doi.org/10.1111/php.13185

Lv, S., Dudek, D. M., Cao, Y., Balamurali, M. M., Gosline, J., & Li, H. (2010). Designed biomaterials to mimic the mechanical properties of muscles. *Nature, 465*(7294), 69–73. https://doi.org/10.1038/nature09024

Meng, X., Lu, Y., Gao, Y., Cheng, S., Tian, F., Xiao, Y., & Li, F. (2021). Chitosan/alginate/hyaluronic acid polyelectrolyte composite sponges crosslinked with genipin for wound dressing application. *International Journal of Biological Macromolecules, 182*, 512–523. https://doi.org/10.1016/j.ijbiomac.2021.04.044

Mi, F. L., Tan, Y. C., & Liang, H. C. (2001). In vitro evaluation of a chitosan membrane cross-linked with genipin. *Journal of Biomaterials Science, Polymer Edition, 12*(8), 835–850. https://doi.org/10.1163/156856201753113051

Mortazavi, V., Mehdikhani Nahrkhalaji, M., Fathi, M. H., Mousavi, S. B., & Nasr Esfahani, B. (2010). Antibacterial effects of sol-gel-derived bioactive glass nanoparticle on aerobic bacteria. *Journal of Biomedical Materials Research - Part A, 94*(1), 160–168. https://doi.org/10.1002/jbm.a.32678

Murtas, S., Capuani, G., Dentini, M., Manetti, C., Masci, G., Massimi, M., Miccheli, A., & Crescenzi, V. (2005). Alginate beads as immobilization matrix for hepatocytes perfused in a bioreactor: A physico-chemical characterization. *Journal of Biomaterials Science, Polymer Edition, 16*(7), 829–846. https://doi.org/10.1163/1568562054255718

Naik, R. R., & Singamaneni, S. (2017). Introduction: Bioinspired and biomimetic materials. *Chemical Reviews, 117*(20), 12581–12583. https://doi.org/10.1021/acs.chemrev.7b00552

Ng, W. L., Yeong, W. Y., & Naing, M. W. (2016). Polyelectrolyte gelatin-chitosan hydrogel optimized for 3D bioprinting in skin tissue engineering. *International Journal of Bioprinting, 2*(1), 53–62. https://doi.org/10.18063/IJB.2016.01.009

Nicu, R., Ciolacu, F., & Ciolacu, D. E. (2021). Advanced functional materials based on nanocellulose for pharmaceutical/medical applications. *Pharmaceutics, 13*(8), 1–57.

O'Brien, F. J. (2011). Biomaterials & scaffolds for tissue engineering. *Materials Today, 14*(3), 88–95. https://doi.org/10.1016/S1369-7021(11)70058-X

Patil, T., Saha, S., & Biswas, A. (2017). Preparation and characterization of HAp coated chitosan-alginate PEC porous scaffold for bone tissue engineering. *Macromolecular Symposia, 376*(1), 1–9. https://doi.org/10.1002/masy.201600205

Patterson, J., Martino, M. M., & Hubbell, J. A. (2010). Biomimetic materials in tissue engineering. *Materials Today, 13*(1–2), 14–22. https://doi.org/10.1016/S1369-7021(10)70013-4

Pellegrino, L., Cocchiola, R., Francolini, I., Lopreiato, M., Piozzi, A., Zanoni, R., … Martinelli, A. (2017). Taurine grafting and collagen adsorption on PLLA films improve human primary chondrocyte adhesion and growth. *Colloids and Surfaces B: Biointerfaces, 158*, 643–649. https://doi.org/10.1016/j.colsurfb.2017.07.047

Picardo, M., & Dell'Anna, M. L. (2010). Oxidative stress. *Vitiligo*, 231–237. https://doi.org/10.1007/978-3-540-69361-1_27

Potaś, J., Szymańska, E., & Winnicka, K. (2020). Challenges in developing of chitosan – Based polyelectrolyte complexes as a platform for mucosal and skin drug delivery. *European Polymer Journal, 140*(September), Article 110020. https://doi.org/10.1016/j.eurpolymj.2020.110020

Qin, Y. (2008). Alginate fibres: An overview of the production processes and applications in wound management. *Polymer International, 57*, 171–180. https://doi.org/10.1002/pi

Radwan-Pragłowska, J., Piątkowski, M., Janus, Ł., Bogdał, D., Matysek, D., & Cablik, V. (2018). Microwave-assisted synthesis and characterization of antioxidant chitosan-based aerogels for biomedical applications. *International Journal of Polymer Analysis and Characterization, 23*(8), 721–729. https://doi.org/10.1080/1023666X.2018.1504471

Raeisdasteh Hokmabad, V., Davaran, S., Ramazani, A., & Salehi, R. (2017). Design and fabrication of porous biodegradable scaffolds: A strategy for tissue engineering. *Journal of Biomaterials Science, Polymer Edition, 28*(16), 1797–1825. https://doi.org/10.1080/09205063.2017.1354674

Raj, S., Kumar Sharma, P., & Malviya, R. (2018). Pharmaceutical and tissue engineering applications of polyelectrolyte complexes. *Current Smart Materials, 3*(1), 21–31. https://doi.org/10.2174/2405465803666180409130241

Reys, L. L., Silva, S. S., Pirraco, R. P., Marques, A. P., Mano, J. F., Silva, T. H., & Reis, R. L. (2017). Influence of freezing temperature and deacetylation degree on the performance of freeze-dried chitosan scaffolds towards cartilage tissue engineering. *European Polymer Journal, 95*(August), 232–240. https://doi.org/10.1016/j.eurpolymj.2017.08.017

Russo, R., Malinconico, M., & Santagata, G. (2007). Effect of cross-linking with calcium ions on the physical properties of alginate films. *Biomacromolecules, 8*(10), 3193–3197. https://doi.org/10.1021/bm700565h

Sæther, H. V., Holme, H. K., Maurstad, G., Smidsrød, O., & Stokke, B. T. (2008). Polyelectrolyte complex formation using alginate and chitosan. *Carbohydrate Polymers, 74*(4), 813–821. https://doi.org/10.1016/j.carbpol.2008.04.048

Shaik, M. M., Dapkekar, A., Rajwade, J. M., Jadhav, S. H., & Kowshik, M. (2019). Antioxidant-antibacterial containing bi-layer scaffolds as potential candidates for management of oxidative stress and infections in wound healing. *Journal of Materials Science: Materials in Medicine, 30*(1), 1–13. https://doi.org/10.1007/s10856-018-6212-8

Shaik, M. M., & Kowshik, M. (2019). Ellagic acid containing collagen-chitosan scaffolds as potential antioxidative bio-materials for tissue engineering applications. *International Journal of Polymeric Materials and Polymeric Biomaterials, 68*(4), 208–215. https://doi.org/10.1080/00914037.2018.1443927

Silvestro, I., Francolini, I., Di Lisio, V., Martinelli, A., Pietrelli, L., Scotto, A., … Piozzi, A. (2020). Preparation and characterization of TPP-chitosan crosslinked Sca ff olds for tissue engineering. *Materials, 13*(3577), 1–15.

Silvestro, I., Sergi, R., D'Abusco, A. S., Mariano, A., Martinelli, A., Piozzi, A., & Francolini, I. (2021). Chitosan scaffolds with enhanced mechanical strength and elastic response by combination of freeze gelation, photo-crosslinking and freeze-drying. *Carbohydrate Polymers, 267*(May), Article 118156. https://doi.org/10.1016/j.carbpol.2021.118156

Simon, H. U., Haj-Yehia, A., & Levi-Schaffer, F. (2000). Role of reactive oxygen species (ROS) in apoptosis induction. *Apoptosis, 5*(5), 415–418. https://doi.org/10.1023/A:1009616228304

Slomkowski, S. (2007). Biodegradable polyesters for tissue engineering. *Macromolecular Symposia, 253*, 47–58. https://doi.org/10.1002/masy.200750706

Sood, A., Gupta, A., & Agrawal, G. (2021). Recent advances in polysaccharides based biomaterials for drug delivery and tissue engineering applications. *Carbohydrate Polymer Technologies and Applications, 2*(March), Article 100067. https://doi.org/10.1016/j.carpta.2021.100067

Stratton, S., Shelke, N. B., Hoshino, K., Rudraiah, S., & Kumbar, S. G. (2016). Bioactive polymeric scaffolds for tissue engineering. *Bioactive Materials, 1*(2), 93–108. https://doi.org/10.1016/j.bioactmat.2016.11.001

Sun, Z., Shi, C., Wang, X., Fang, Q., & Huang, J. (2017). Synthesis, characterization, and antimicrobial activities of sulfonated chitosan. *Carbohydrate Polymers, 155*, 321–328. https://doi.org/10.1016/j.carbpol.2016.08.069

Suo, H., Zhang, D., Yin, J., Qian, J., Wu, Z. L., & Fu, J. (2018). Interpenetrating polymer network hydrogels composed of chitosan and photocrosslinkable gelatin with enhanced mechanical properties for tissue engineering. *Materials Science and Engineering C, 92*(July), 612–620. https://doi.org/10.1016/j.msec.2018.07.016

Tchobanian, A., Van Oosterwyck, H., & Fardim, P. (2019). Polysaccharides for tissue engineering: Current landscape and future prospects. *Carbohydrate Polymers, 205*(October 2018), 601–625. https://doi.org/10.1016/j.carbpol.2018.10.039

Thein-Han, W. W., & Misra, R. D. K. (2009). Biomimetic chitosan-nanohydroxyapatite composite scaffolds for bone tissue engineering. *Acta Biomaterialia, 5*(4), 1182–1197. https://doi.org/10.1016/j.actbio.2008.11.025

Tyagi, N., Gambhir, K., Kumar, S., Gangenahalli, G., & Verma, Y. K. (2021). Interplay of reactive oxygen species (ROS) and tissue engineering: A review on clinical aspects of ROS-responsive biomaterials. *Journal of Materials Science, 56*(30). https://doi.org/10.1007/s10853-021-06338-7 (Springer US).

Vikingsson, L., Claessens, B., Gómez-Tejedor, J. A., Gallego Ferrer, G., & Gómez Ribelles, J. L. (2015). Relationship between micro-porosity, water permeability and mechanical behavior in scaffolds for cartilage engineering. *Journal of the Mechanical Behavior of Biomedical Materials, 48*, 60–69. https://doi.org/10.1016/j.jmbbm.2015.03.021

Vunain, E., Mishra, A. K., & Mamba, B. B. (2017). 1 – Fundamentals of chitosan for biomedical applications. In , *Vol. 1. Chitosan based biomaterials: Volume 1: Fundamentals*. Elsevier. https://doi.org/10.1016/B978-0-08-100230-8.00001-7.

Wahba, M. I. (2020). Enhancement of the mechanical properties of chitosan. *Journal of Biomaterials Science, Polymer Edition, 31*(3), 350–375. https://doi.org/10.1080/09205063.2019.1692641

Wang, C., Yu, Y., Chen, H., Zhang, S., Wang, J., & Liu, C. (2019). Construction of cytokine reservoirs based on sulfated chitosan hydrogels for the capturing of VEGF in situ. *Journal of Materials Chemistry B, 7*(11), 1882–1892. https://doi.org/10.1039/C8TB02895H

Xu, H. H. K., & Simon, C. G. (2005). Fast setting calcium phosphate-chitosan scaffold: Mechanical properties and biocompatibility. *Biomaterials, 26*(12), 1337–1348. https://doi.org/10.1016/j.biomaterials.2004.04.043

Xu, Y., Xia, D., Han, J., Yuan, S., Lin, H., & Zhao, C. (2017). Design and fabrication of porous chitosan scaffolds with tunable structures and mechanical properties. *Carbohydrate Polymers, 177*(August), 210–216. https://doi.org/10.1016/j.carbpol.2017.08.069

Yang, B., Li, X. Y., Shi, S., Kong, X. Y., Guo, G., Huang, M. J., … Qian, Z. Y. (2010). Preparation and characterization of a novel chitosan scaffold. *Carbohydrate Polymers, 80*(3), 860–865. https://doi.org/10.1016/j.carbpol.2009.12.044

Zhao, J., Griffin, M., Cai, J., Li, S., Bulter, P. E. M., & Kalaskar, D. M. (2016). Bioreactors for tissue engineering: An update. *Biochemical Engineering Journal, 109*, 268–281. https://doi.org/10.1016/j.bej.2016.01.018

Zheng, H. (1997). Interaction mechanism in sol-gel transition of alginate solutions by addition of divalent cations. *Carbohydrate Research, 302*(1–2), 97–101. https://doi.org/10.1016/S0008-6215(97)00114-6

Zheng, X., Zhang, P., Fu, Z., Meng, S., Dai, L., & Yang, H. (2021). Applications of nanomaterials in tissue engineering. *RSC Advances, 11*(31), 19041–19058. https://doi.org/10.1039/d1ra01849c

Zhou, H., Qian, J., Wang, J., Yao, W., Liu, C., Chen, J., & Cao, X. (2009). Enhanced bioactivity of bone morphogenetic protein-2 with low dose of 2-N, 6-O-sulfated chitosan in vitro and in vivo. *Biomaterials, 30*(9), 1715–1724. https://doi.org/10.1016/j.biomaterials.2008.12.016